

## A Database of 2MASS Near-Infrared Colors of Magellanic Cloud Star Clusters

Peter M. Pessev, Paul Goudfrooij, Thomas H. Puzia, & Rupali Chandar<sup>1</sup>

*Space Telescope Science Institute*

*3700 San Martin Drive, Baltimore, MD 21218, USA*

pessev, goudfroo, tpuzia, rupali@stsci.edu

### ABSTRACT

The (rest-frame) near-IR domain contains important stellar population diagnostics and is often used to estimate masses of galaxies at low as well as high redshifts. However, many stellar population models are still relatively poorly calibrated in this part of the spectrum. To allow an improvement of this calibration we present a new database of integrated near-infrared  $JHK_s$  magnitudes for 75 star clusters in the Magellanic Clouds, using the 2-Micron All-Sky Survey (2MASS). The majority of the clusters in our sample have robust age and metallicity estimates from color-magnitude diagrams available in the literature, and populate a range of ages from 10 Myr to 15 Gyr and a range in  $[\text{Fe}/\text{H}]$  from  $-2.17$  to  $+0.01$  dex. A comparison with matched star clusters in the 2MASS Extended Source Catalog (XSC) reveals that the XSC only provides a good fit to the *unresolved* component of the cluster stellar population. We also compare our results with the often-cited single-channel  $JHK$  photometry of Persson et al. (1983), and find significant differences, especially for their  $30''$ -diameter apertures up to  $\sim 2.5$  mag in the  $K$ -band, more than 1 mag in  $J-K$ , and up to 0.5 mag in  $H-K$ . Using simulations to center apertures based on maximum light throughput (as performed by Persson et al.), we show that these differences can be attributed to near-IR-bright cluster stars (e.g., Carbon stars) located away from the true center of the star clusters. The wide age and metallicity coverage of our integrated  $JHK_s$  photometry sample constitutes a fundamental dataset for testing population synthesis model predictions, and for direct comparison with near-IR observations of distant stellar populations.

---

<sup>1</sup>Present Address: Department of Physics and Astronomy, Johns Hopkins University, 3400 N. Charles Street, Baltimore, MD 21218

## 1. Introduction

Much of our understanding of galaxy formation and evolution comes from studying stellar populations in different galaxy types, both in the present and early universe. Two key parameters of stellar systems which are widely used throughout the literature are mean ages and metallicities. Ages and/or metallicities of stellar systems in photometric surveys are estimated by comparing measured integrated colors with the predictions of evolutionary synthesis models (e.g. Bruzual & Charlot 1993, 2003; Worthey 1994; Vazdekis 1999; Maraston 1998, 2005). These models utilize stellar isochrone libraries, which are synthesized in appropriate combinations to represent stellar systems at different ages and metallicities. There are however, two important limitations inherent to these models. First, the stellar libraries themselves contain mostly stars in the solar neighborhood, which have a star formation history that is not necessarily typical for extragalactic populations (e.g., relatively little variation in chemical composition). Second, the synthesis models oversimplify the more rapid (but very luminous) phases of stellar evolution (e.g., thermally pulsing asymptotic giant branch stars). Given the very fundamental nature of the information that is derived by comparison with these models, it is imperative that population synthesis models be as accurate as possible.

Simple stellar population (SSP) models are empirically calibrated to observations of real star clusters for which ages and metallicities are known from independent analysis, e.g., color-magnitude diagrams (e.g. Bruzual et al. 1997; Maraston et al. 2003). While much of the work to date has been carried out at optical wavelengths, the near-infrared (NIR) regime contains some very important diagnostics for deriving basic properties of stellar systems. In fact, this wavelength regime has been shown to be very important for sorting out the effects of age and metallicity, particularly in stellar populations older than about 300 Myr (e.g. Goudfrooij et al. 2001; Puzia et al. 2002; Hempel & Kissler-Patig 2004). Due to recent advances in the instrumentation and detector capabilities in the NIR passbands, and considering the focus on the infrared in the next generation of telescopes, it is clear that the accuracy of SSP models in the NIR is going to be even more important in the future.

In this work, we present integrated NIR colors of a large sample of star clusters in the Large and Small Magellanic Cloud (hereafter LMC and SMC). We make use of data from the Two Micron All Sky Survey (2MASS Skrutskie et al. 1997), which offers uniform, high-quality imaging of the entire sky in three bands,  $J$  ( $1.25 \mu\text{m}$ ),  $H$  ( $1.65 \mu\text{m}$ ), and  $K_s$ <sup>1</sup> ( $2.16 \mu\text{m}$ ). Our main goal is to provide a new database of intrinsic NIR magnitudes and colors of clusters with well-known ages and metallicities from deep color-magnitude diagrams (CMDs),

---

<sup>1</sup>For a description of the "K short" ( $K_s$ ) band, see Persson et al. (1998).

that can be utilized as a calibration dataset by existing and future generation SSP models. The clusters in the Magellanic Clouds are very suitable for addressing this issue. They cover a wide range of ages, and they are close enough for detailed CMD studies using the Hubble Space Telescope (*HST*), (in some cases also with large telescopes from the ground). Unlike the globular cluster system (GCS) of our Galaxy, there are a significant number of objects with intermediate ages (0.3–3 Gyr) in the LMC and SMC. The integrated-light properties of these systems are affected strongly by AGB stars which are extremely luminous in the NIR, and their contribution to the light in that part of the spectrum is largely underestimated by most existing SSP models (see Maraston 2005).

The measurement of integrated magnitudes and colors of star clusters in the Magellanic Clouds is complicated by several factors. One problem is that of accurate centering of the aperture. Many of these clusters are superposed onto a relatively high surface density of stars associated with the LMC or SMC, and some have a rather irregular field distribution and/or are not particularly symmetric due to the superposition of bright stars (be it supergiants or AGB stars, associated with the cluster itself, those from the body of the LMC or SMC, or Galactic foreground stars). On the other hand, it should be recognized that the use of 2-dimensional imagery renders these problems much less severe than they were for often-cited previous studies which used single-channel photometers and diaphragms which were centered either by eye or by maximum throughput.

The present study is complementary to the information about Magellanic Cloud clusters in 2MASS Extended Source Catalog (XSC Jarrett et al. 2000) in three ways: (*i*) providing photometry for a set of clusters that are not present in the 2MASS XSC; (*ii*) we take into account the flux from the point sources associated with the star clusters, which are rejected by the XSC pipeline (see §3.2 for details); (*iii*) better sampling of the curves of growth with a step of 1", instead of 11 fixed circular apertures.

This paper is organized as follows: Section 2 describes the sample selection, data acquisition and reduction. The results, including comparison with previous works and 2MASS XSC are presented in §3. Finally, a summary is provided in §4.

## 2. Near-Infrared Data

### 2.1. Sample selection

Our original sample of star clusters was adopted from Mackey & Gilmore (2003a,b), and most have accurate CMD ages and metallicities from the literature. We particularly pay attention to the largest possible coverage of the available age/metallicity parameter

space. In addition, we select intermediate-age and young clusters which have no known counterparts in the Milky Way globular cluster system. The adopted distance moduli are  $m - M = 18.89$  and  $m - M = 18.50$  for the SMC (Harries et al. 2003) and LMC (Alves 2004) respectively. Basic information for all objects is provided in Tables 1 and 2 (respectively for star clusters in the SMC and LMC).

The young SMC cluster NGC 176 was included in the original list, but after inspection of the 2MASS images it became clear that the NIR data is too shallow to derive reliable integrated colors. R136 in LMC, the youngest object in the preliminary selection, is embedded in an extensive emission region that would affect the results of the integrated photometry. We decided not to include these two clusters in the final list.  $J$ ,  $H$ , and  $K_s$  postage stamp images of representative objects in our sample are presented in Figure 1 (SMC) and 2 (LMC).  $V$ -band frames for the majority of the SMC objects, included in this work, can be found in Hill & Zaritsky (2005).

## 2.2. 2MASS Atlas Images

The 2MASS Atlas Images originate from 6°-long survey scans using an effective integration time of 7.8 seconds per tile.  $J$ ,  $H$ , and  $K_s$  images were retrieved using the 2MASS interactive image service<sup>2</sup>. The queries were usually sent by object name and in some cases, when the name qualifier was not recognized, by coordinates. In most cases an object could be found on several sets of frames, allowing us to choose the best one, taking into account the relative position of the cluster and the characteristics of each field. Tables 3 and 4 provide information on the Atlas Images, selected for our study, for SMC and LMC clusters, respectively. Column 2 in these tables provides the number of different sets of images retrieved for each object.

The raw survey data was reduced at the Infrared Processing and Analysis Center with the pipeline specifically developed for 2MASS. The imaging data is resampled to 1''/ pixel, calibrated to one second integration time and contain both the astrometric solution and the photometric zero points for each individual Atlas Image (Cutri et al. 2003). The astrometric solutions are obtained in the International Celestial Reference System via the Tycho-2 Reference Catalog. Taking into account the higher value of the extended source uncertainty (Cutri et al. 2003), all cluster positions derived in the present work were rounded to the nearest half pixel (0''.5).

---

<sup>2</sup><http://irsa.ipac.caltech.edu/applications/2MASS/IM/interactive.html>

The photometric zero points are based on observations of fields, covering the NIR standards from the list of Persson et al. (1998) or the UKIRT group of faint, equatorial NIR standard stars (Casali & Hawarden 1992). The solution is derived independently for each band and minimizes the residuals by a least square fit of the zero point, airmass, and atmospheric extinction (Nikolaev et al. 2000). The distributions of the zero point differences for all standard fields in all survey nights turned out to be Gaussian with RMS residual values of 0.011, 0.007 and 0.007 magnitudes in  $J, H$  and  $K_s$ , respectively (Cutri et al. 2003). These values are added in quadrature to the photometric errors in this work.

### 2.3. Data analysis

In order to measure the integrated cluster magnitudes, the following multistep procedure was applied to each object of the sample: *(i)* PSF-fitting photometry of the point sources; *(ii)* determination of the center position for the integrated curve of growth photometry; *(iii)* subtraction of the background/foreground point source luminosity function (LF) from the LF of the cluster field; *(iv)* integrated photometry of the total, background-subtracted and unresolved component of the object in each survey band; *(v)* calculation of the photometric errors for each measurement aperture.

For basic data analysis we use the suite of IRAF<sup>3</sup> tasks and perform DAOPHOTII/ALLSTAR photometry (Stetson 1987) on each frame. Typically several bright and well-isolated stars were used to construct the PSF for each frame. As this is only an intermediate stage in the process of deriving the total integrated cluster magnitudes, aperture corrections are not applied at this point. The ALLSTAR routine is used to produce frames on which individual stars are removed after being measured. We will refer to these frames as "residual frames", which will later be used to study the part of the cluster stellar population not resolved in the 2MASS images.

In many cases the coordinates taken from cluster catalogs in the literature do not provide an accurate position for the center of individual clusters. We applied a simple and robust method to derive the centers in the present paper. The original frames and the residual frames in each survey band were smoothed with a large Gaussian kernel. The size of the kernel varied as a function of the cluster size on the  $J$  frames, where the sensitivity of 2MASS reaches its peak. The maximum flux values on an image subsection of the smoothed images

---

<sup>3</sup>IRAF is distributed by the National Optical Astronomical Observatory, which is operated by the Associations of Universities for Research in Astronomy Inc., under cooperative agreement with the National Science Foundation.

in each of the survey bands, derived by the IRAF task MINMAX were used to determine the individual cluster centers in  $J$ ,  $H$ , and  $K_s$ . They were later averaged to derive the final center coordinates that were used for the integrated photometry in the present paper. Possible sources of confusion (e.g., bright stars outside the cluster area, present on the original Atlas frames) were avoided by performing the procedure described earlier on an image subsection, covering the rough cluster position on the smoothed images. We point out that the cluster images in Figures 1 and 2 are extracted from the 2MASS frames, using the centers derived with this procedure. Each image covers  $200'' \times 200''$  and is representative of the size of the largest aperture used to measure integrated cluster magnitudes.

In a few cases the object was situated close to the edge of the Atlas frame. This is not a serious problem for most clusters because we were still able to sample the flux out to large enough radii to derive the total integrated magnitudes. One exception was Lindsay 1 which was split almost equally between two sets of frames. The special data reduction procedure, applied to this object is described in Section 2.7 below.

## 2.4. Stellar Background Subtraction

To estimate the contamination of our globular cluster fields by foreground stars and stars associated with the body of the LMC or SMC we used the portion of the frames outside of the largest aperture used for integrated-light photometry, (typically  $100''$ ). The luminosity function (LF) for the point sources in these background regions was scaled to the cluster area used for photometry. This was statistically subtracted from the point source LF measured inside the photometric radius. The area of the background regions slightly varied as a function of the largest aperture size, but even in the case of  $100''$  aperture radii it was more than 15 times larger than the photometry area. In this way we achieve a good estimate of the background/foreground contamination, one which is much less affected by local stellar variations and therefore superior to just subtracting a normalized background flux from a neighboring annulus. To illustrate our procedure, in Figure 3 we show the LFs of the background, cluster, and the cleaned LF after the background subtraction, for the heavily contaminated cluster NGC 330.

In cases where bright stars (not sampled by the field star LF) are present in the cluster aperture, after the background subtraction we are utilizing their ALLSTAR PSF magnitudes and corresponding colors to make a rough estimation of the spectral and luminosity class using the work of Ducati et al. (2001). The visual magnitudes of these objects were recovered using the visual – infrared colors from the same study for a certain spectral and luminosity class. The results were compared with the age of the cluster and the expected absolute

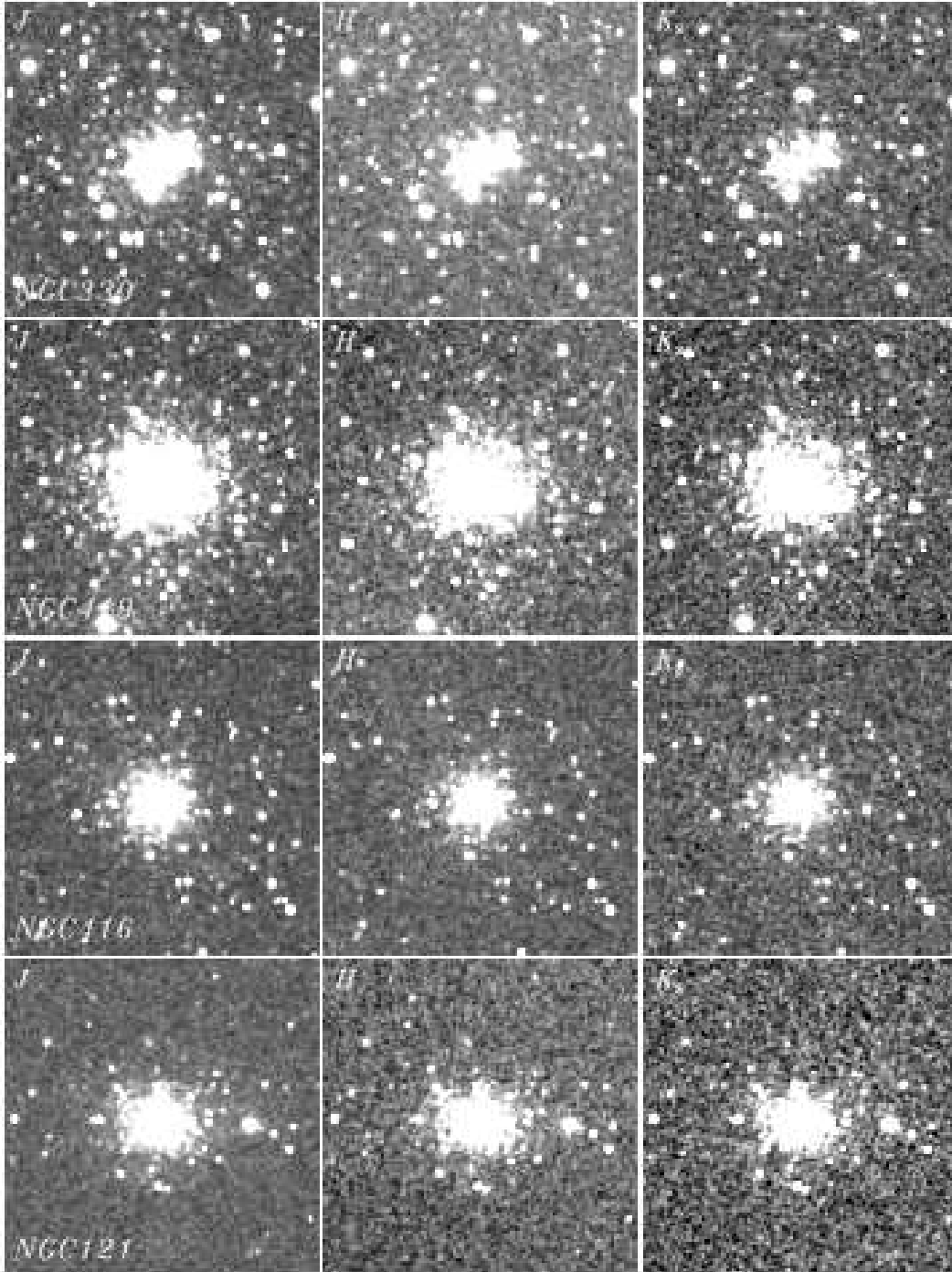


Fig. 1.—  $J, H,$  and  $K_s$  images of 4 SMC clusters. Each image is  $200'' \times 200''$ , centered on the cluster position derived in the present paper. North is up, East is to the left. The curves of growth for each of these objects can be found on Figure 8.

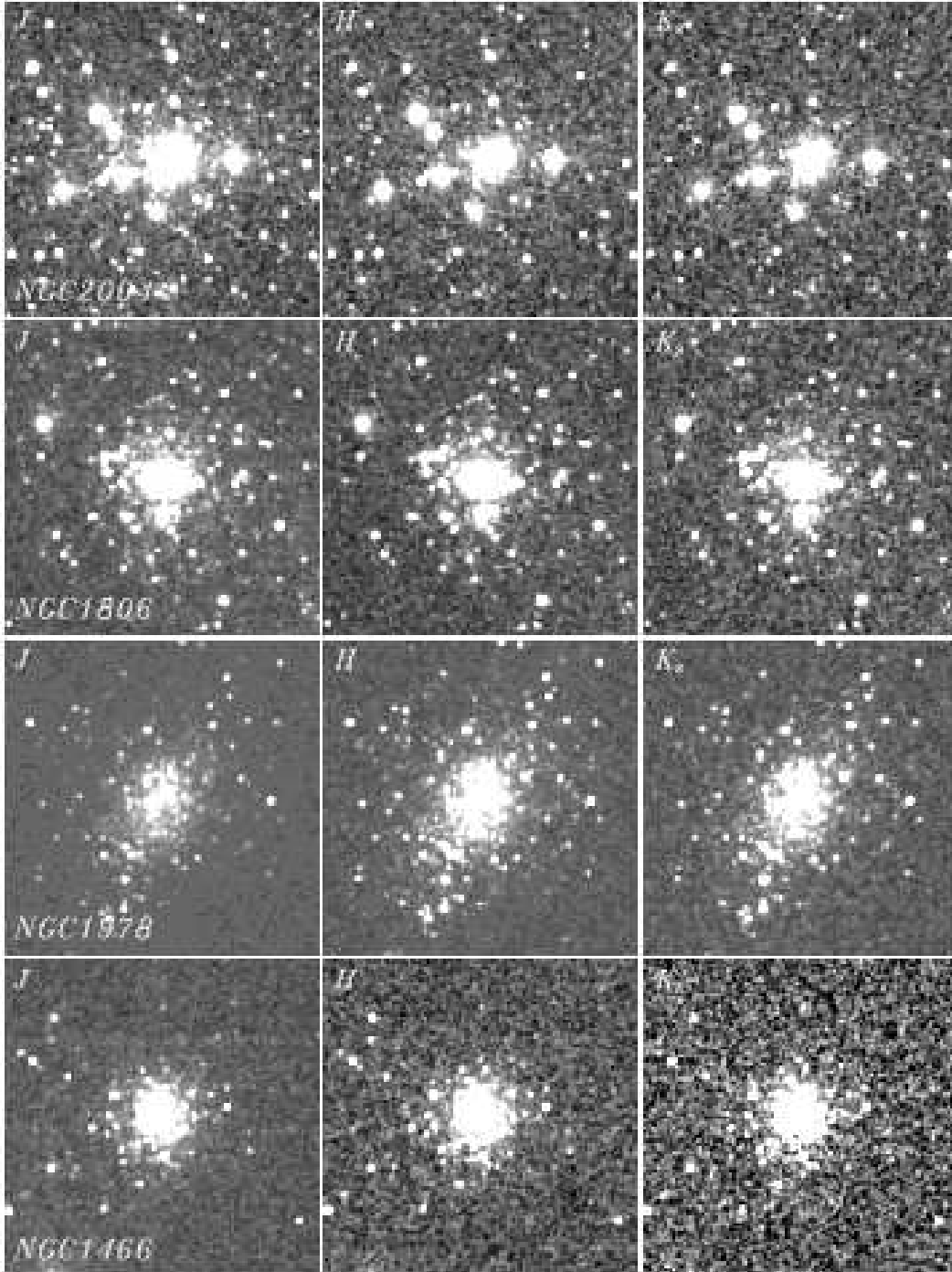


Fig. 2.—  $J, H,$  and  $K_s$  images of 4 LMC clusters. Each image is  $200'' \times 200''$ , centered on the cluster position derived in the present paper. North is up, East is to the left. The curves of growth for each of these objects can be found on Figure 9.



visual magnitudes of these stars at the distance to SMC or LMC. If there was a discrepancy between the measured and expected magnitudes or if such stars were unlikely to be found in a cluster with the given age, they were subtracted. There are several examples of this procedure described in Section 2.7.

## 2.5. Integrated Cluster Photometry

The aperture photometry of the clusters was performed with IRAF APPHOT package on a set of three residual images in each survey band. The images are a result by the application of DAOPHOT/ALLSTAR and the IRAF SUBSTAR procedure on the original atlas frames. On the first of them all detected point sources were removed (actually this is the output residual image from ALLSTAR), on the second the LF of the background field was subtracted from the cluster area using SUBSTAR with a exclude file, containing the stars remaining after the statistical subtraction, the third image contained all the point sources within the photometry aperture. The images were used to measure the flux from the unresolved component, background subtracted and the total flux from the object, using a set of apertures ranging from 1" to 100" in radius with a step size of 1". We computed curves of growth for all sample globular clusters in the three survey bands. The sky background level in each frame was estimated in a sky annulus encircling our largest aperture with width at least 10 pixels. The exclusion of the stars outside of the largest aperture prior to the final integrated photometry is providing a better estimate of the sky background. In those cases where the cluster was situated close to the frame edge, we used the largest aperture possible, and the background levels were measured in a nearby region that matched or exceeded the equivalent area of a full background annulus circle.

For each aperture the error introduced by the stochastic fluctuations in the stellar population of the foreground/background was estimated. We computed the luminosity function (LF) of objects outside each photometry aperture for each particular object. The corresponding flux was integrated over the entire LF and the standard deviation of stellar counts were calculated in bins of  $\Delta m = 1$  mag. These values were then normalized to the area used for the cluster photometry. Bright stars close to saturation were identified on the images and excluded from the photometry prior to the procedures described above. The error values listed in Tables 5 and 5 in each survey band are the quadrature sum of the photometry errors from APPHOT, the 2MASS zero point errors and the calculated background stochastic fluctuations. In general, the errors of our photometry increase as a function of aperture radius and depend on background properties.

Example curves of growth of the photometry for the SMC cluster NGC411 and LMC

cluster NGC 2231 are presented in Figures 4 and 5, respectively. The solid line shows the magnitude of the cluster after background subtraction. The estimated errors due to stochastic background fluctuations are overplotted with dotted lines. The dashed curve represents the total flux from the cluster (without background subtraction), and the unresolved component is plotted with dot-dashed lines. NGC 2231 in Figure 5 also illustrates what could be the effect on the integrated magnitudes of the cluster if there is improper handling of the background subtraction. This cluster lie in a region of relatively high apparent stellar density and there are several bright stars present. The stochastic fluctuations of the stellar background show the possibility of a severe overestimation of the cluster total magnitude if the influence of the bright stellar objects is not taken into account. Note that the error values in Table 5 are calculated with the bright stars excluded from the background LF. Integrated magnitudes and photometric curves of growth for all star clusters analyzed in this study are available upon request from the first author.

## 2.6. Extinction correction

In order to determine the intrinsic magnitudes and colors of our sample clusters, the measurements must be corrected for the effect of extinction. Cluster extinction values were obtained from three independent studies: Burstein & Heiles (1982), Schlegel et al. (1998), and the Magellanic Clouds Photometric Survey (MCPS, Zaritsky et al. 1997): see Zaritsky et al. (2002) for SMC and Zaritsky et al. (2004) for LMC. The study by Burstein & Heiles is based on maps of the HI emission, while the Schlegel et al. maps use IRAS/DIRBE data of the FIR sky emission. The corrections provided by Schlegel et al. (1998) are superior to those of Burstein & Heiles (1982), because of the improved spatial resolution and the fact that they estimate the extinction from the dust properties directly, not using HI as an intermediate agent. But there is an important caveat - the Schlegel et al. maps are highly uncertain in the inner regions of the Clouds because their temperature structure wasn't sufficiently resolved by DIRBE. The most recent development in Magellanic Clouds extinction work is the MCPS data. This survey covers the central  $4^\circ \times 4^\circ$  of the SMC and  $8^\circ \times 8^\circ$  of the LMC in *UBVI*. The limiting magnitude of the MCPS maps (set primarily by crowding) is  $V = 21$  mag. However, these maps cover only the inner body of the Magellanic Clouds and extinction information for star clusters located in the outer regions is not available.

Extinction estimates based on HI emission and IRAS/DIRBE dust maps were retrieved for all objects from NASA/IPAC Extragalactic Database (NED). The values from MCPS

were retrieved using the online tools available on the webpage of the project<sup>4</sup>. The MCPS maps provide a statistical approach to the extinction: stellar atmosphere models are fit to their measured *UBVI* magnitudes of all the stars in an user defined search radius with good quality photometry and good model fits (Zaritsky 1999). The distribution of the extinction values is built and the result of the mean extinction and  $\sigma_{ext}$  of the distribution is given. There are different options available, but for the current work we chose to use the estimates based on "cool" stars ( $T \leq 10^4$  K) in the search radius. Since cool stars are more homogeneously distributed than hot stars, extinction measurements from cool stars should provide a more representative estimate of the true extinction value. The extinction map of the central region of the LMC, showing all the objects with estimates available from the three studies is presented in Figure 6. Generally the values from Burstein & Heiles (1982) and Schlegel et al. (1998) are in good agreement, but, in most cases, lower than those derived from Zaritsky et al. (2004). Using a search radius of  $2'$ , which is slightly larger than our largest photometry aperture, we achieve a robust estimate of the extinction towards a specific object.

We use the extinction values based on the MCPS maps. In those cases where no MCPS data is available, we adopt a typical extinction value, derived from all objects with extinction estimates from MCPS. These mean values were derived by fitting the extinction distribution for 40 LMC and 9 SMC clusters by a gaussian (see Figure 7). The adopted values are:  $A_B = 0.52 \pm 0.02$  and  $A_V = 0.39 \pm 0.02$  for LMC,  $A_B = 0.22 \pm 0.01$  and  $A_V = 0.18 \pm 0.01$  for SMC. They are higher than the mean values from Schlegel et al., which are  $A_B = 0.32 \pm 0.05$  and  $A_V = 0.16 \pm 0.03$  for LMC and SMC, respectively. This result is consistent with the fact that the extinction values for LMC and SMC listed in Schlegel et al. (1998) only provide lower limits: They only account for Galactic dust, whereas the dust in the Clouds is not taken into consideration.

We adopt the extinction law of Bessell & Brett (1988).

To account for the younger stellar population in objects in our sample with  $\log(age) < 8.3$ , we are using the extinction values based on all stars. This approach is providing a better estimate than "hot" star ( $T \leq 10^4$  K) alone, because it is reducing the influence of the relatively shallow MCPS *U* band photometry.

---

<sup>4</sup><http://ngala.as.arizona.edu/dennis/mcsurvey.html>

## 2.7. Notes on individual objects

There are a few cases in which the data reduction and photometry differed slightly from the procedure described above. Additional remarks for these clusters are provided below.

**NGC 121** There is a relatively bright star located  $\sim 60''$  W from the center of the cluster. An inspection of 2MASS and optical images (from SIMBAD<sup>5</sup>) showed that it is most likely a foreground star superposed on the cluster. Its magnitudes from ALLSTAR output files are  $J = 10.78$ ,  $H = 10.22$  and  $K_s = 10.11$ . The extinction correction values are taken from Burstein & Heiles (1982) and Schlegel et al. (1998) (we discuss extinction corrections in detail in Section 2.6). They are  $A_B = 0.15$  and  $0.16$ , respectively, and we use their mean in this analysis. The measured colors are:  $(J - H)_0 = 0.55$ ,  $(H - K_s)_0 = 0.104$ ,  $(J - K_s)_0 = 0.65$ . Comparing with the results of Ducati et al. (2001) for intrinsic NIR colors of stars shows that its colors are consistent with a K main-sequence, G giant or supergiant star. In the latter case, rough derivation of the absolute visual magnitude at the distance of SMC gives  $M_V \approx -7.5$  mag. This is consistent with the star being a supergiant, but it is not likely that such an object is found in a  $\sim 12$  Gyr old star cluster. Therefore, we assume that the star belongs to the foreground and subtract it prior to the final cluster photometry.

**NGC 339** This object is relatively close to the edge of the Atlas Image. The radius of the largest aperture used for photometric measurements is  $90''$ . In all cases, when the maximal size of the apertures was smaller than the typical value of  $200''$ , the last entries for the particular object in Table 5 or 6 are the magnitudes measured in the largest apertures used.

**NGC 419** There is a bright star in the aperture area  $\sim 90''$  SSE from the center used for photometry. It is clearly visible on the optical frames retrieved from SIMBAD. Given its colors of  $J - K_s = 0.410$  and  $H - K_s = 0.004$  we conclude that it is most likely a foreground object and subtract it prior to the final measurements.

**NGC 458** This young cluster is barely visible in the 2MASS frames, in particular in  $H$  and  $K_s$  where the infrared sky background is significantly higher. The curves of growth in these bands start to decline for aperture diameters larger than  $80''$ . We provide integrated magnitudes only up to  $90''$  aperture radius, due to the proximity of this cluster to the edge of the Atlas Image, but the results for the largest radius must be treated with caution.

**Lindsay 1** The cluster was split almost equally between two sets of frames. To derive its integrated magnitudes we could not use the usual centering routine and the center was

---

<sup>5</sup><http://simbad.u-strasbg.fr/>

derived "by eye", accounting for the appearance and position of the cluster on each image. The fluxes from the two halves were measured independently, summed together, and converted into magnitude values. The frames originate from the same scan, acquired on Aug. 8 1998 between 07:03:03.00 and 07:08:51.00 UT. The regions of the sky on these images were observed at 07:03:43.51 and 07:04:01:38 UT one after another. Hence, we averaged the zero points of the frames and used that value for the derivation of the magnitudes. The mean zero points were 20.8522, 20.4090 and 19.8725 in  $J, H$  and  $K_s$ , respectively. The errors of the photometry were estimated in accordance to the described procedure.

**NGC 1711** There is a chain of so-called persistence artifacts in close vicinity to the cluster. These features most likely originate from a bright star outside of the current Atlas Image. Two of them affect the photometry, are located at distances  $\sim 47''$  and  $\sim 66''$  from the center. They are well outside of the unresolved cluster component, and were measured independently on the residual frames. Their flux was subtracted from the affected apertures before calculation of the magnitude values. The rest of the artifacts were avoided by specifying a larger radius for the background annulus. The resulting errors for this cluster were estimated by taking into account the effect of the artifact removal.

**NGC 1754** A bright star is present  $\sim 35''$  SE from the center of the cluster, also clearly visible on the visual frames from SIMBAD. The magnitude values derived from our PSF photometry are  $J=9.31$ ,  $H=8.79$ ,  $K_s=8.68$  mag and the resulting colors:  $J - H = 0.52$ ,  $H - K_s = 0.11$ ,  $J - K_s = 0.63$ . This case is similar to NGC 121 in the SMC. The extinction value towards that object was retrieved from the reddening estimator for LMC on the webpage of MCPS  $A_V = 0.4$ . The corrected colors of the star are then  $(J - H)_0 = 0.48$ ,  $(H - K_s)_0 = 0.08$  and  $(J - K_s)_0 = 0.56$ . These colors best match those of a G4 giant from Ducati et al. (2001). The measured absolute visual magnitude is not compatible with the predictions for a G4 giant. The estimated age of the cluster ( $\sim 15$ Gyr) rules out the possibility that the star is a supergiant. Most likely it is a foreground star and we excluded it from the measurements of the total cluster luminosity.

**NGC 2136** This is one of the most interesting objects in our sample. The cluster is  $\sim 100$  Myr old and there is a "satellite cluster" clearly visible on both visual and near-infrared images  $\sim 80''$  from the central position derived in the present work. The difference between the coordinates retrieved from SIMBAD and the actual center is 166 pixels on the 2MASS  $J$  frame. The object is also off-centered on the optical frame downloaded from the same database as the coordinates. We conclude that the most probable cause of this discrepancy is a mistake in the coordinates listed in SIMBAD. They are given in Table 1, and the values derived for the centering in the present work are listed in Table 6.

There are two bright stars in the set of apertures used to built the curve-of-growth. An

analysis similar to the case of the stars in the field of NGC 121 and NGC 1754 led us to the conclusion that the absolute visual magnitudes differ from those expected for luminous stars of these spectral types. We chose at that point to exclude them from the final photometry.

**NGC 2153** This object was situated too close to the frame edges on all the sets of Atlas Images available. We chose those with the best possible location, but the largest aperture radius is still only  $40''$  before running into the frame edge. However, the cluster is compact and even in that significantly smaller aperture set (compared to that typically used in this work) the curves-of-growth indicate sampling of the entire flux from the object. In fact there is some decline observed in  $H$  for aperture radii larger than  $20''$ . The most likely explanation is local variation in the background, typical for the  $H$  band. Due to the position of the object the background levels were estimated in a region of the sky close to the cluster. We present the results for the complete set of apertures, but the values of  $H$  magnitudes must be treated with caution for radii exceeding  $20''$ .

**SL 842** This compact cluster is barely detected by 2MASS. Photometry is performed with the entire set of apertures, but the results become highly unreliable for aperture radii exceeding  $30''$ . This aperture appears to encompass the measurable flux from the object and these are the results listed in Table 6.

**SL855** The cluster is barely visible on the Atlas Images. The photometry was initially performed with the entire set of apertures. The shape of the curves-of-growth and inspection of the frames led us to adopt a more conservative approach, and we list only the results to aperture radius  $10''$ .

**ESO121-003** The cluster is faint and extended. It is detected by 2MASS, but the curves of growth are noisy.

### 3. Results

The results from the integrated 2MASS photometry of the entire Magellanic Clouds cluster sample are presented in Tables 5 and 6. (The entire tables are available in the electronic version of the journal.) A set of typical NIR  $J$ ,  $H$ , and  $K_s$  curves of growth of four SMC clusters, ranging in age from  $\sim 25$  Myr to  $\sim 12$  Gyr is given on Figure 8. A closer look at the curve of the youngest cluster NGC 330 reveals well visible "bumps". These are bright stars contributing to the total light; these are common for young and some of the intermediate-age clusters, and are most likely massive young supergiants and carbon stars, which emit significant amounts of light in the NIR. Figure 9 presents curves of growth for LMC clusters also covering a representative age range. The corresponding images of these

objects are presented in Figures 1 and 2 for the SMC and LMC, respectively.

The carbon stars present in some intermediate-age clusters are easily distinguished by their colors and luminosity as mentioned by Frogel et al. (1990). They also affect the curve of growth in a typical way, leaving a "fingerprint" of their presence. A good example is the LMC cluster NGC 2190. The curves of growth for this cluster cover the carbon star KDMK6996 (Kontizas et al. 2001) and another candidate carbon star closer to the cluster center (see Figure 10). The features at  $\sim 30''$  and  $60''$  radii are caused by carbon stars entering the aperture. Note the steeper increase of the curve of growth for  $K_s$  compared to those for  $J$  and  $H$ , and the corresponding features in the flux curves. The carbon star identification is based on the magnitudes and colors from their PSF photometry. It is easy to detect the red colors of these objects in the NIR passbands. Their intrinsic colors are expected to be  $(J - H)_0 \approx 1$ ,  $(H - K)_0 \approx 1$  and  $(J - K)_0 \approx 2$  (Ducati et al. 2001).

### 3.1. Comparison with previous studies

We compare our results with the work of Persson et al. (1983) in this section. There are 52 objects in common between our study and their paper: 10 SMC and 42 LMC clusters, respectively. The data in that early work was gathered using three different photo tubes and an InSb detector system, mounted on three different telescopes: The 1-m Swope and 2.5-m du Pont telescopes of the Las Campanas Observatory and the 0.9-m CTIO telescope. The observations of Magellanic Cloud clusters were presented in  $J, H$  and  $K$  filters of the California Institute of Technology infrared photometric system (CIT) (for details see Frogel et al. 1978).

There are several issues that complicate a direct comparison of the obtained results in the two works: *(i)* Due to the use of an iris diaphragm at the du Pont and CTIO telescopes at the time, the aperture diameters were only known to  $\pm 1''$  (Persson et al. 1983). This could lead to uncertainties in the cluster magnitudes and colors. *(ii)* Another serious problem we became aware of during a series of experiments is related to the centering of the cluster. In many cases the diaphragm apertures used by Persson et al. appear to cover the brightest part of the cluster, because their strategy was to maximize the flux through the aperture. This however leaves this technique vulnerable to the effect of stochastic fluctuations of the observed stellar population, in particular for young clusters or clusters that are contaminated by bright stars. Extended clusters without a clear central peak are also difficult to center using this technique. *(iii)* The cross-calibration between the CIT and 2MASS photometric system was only based on three stars with  $(H - K)_{\text{CIT}} > 0.5$  (Carpenter 2001). However, one might expect differences in calibration from CIT  $K$  to 2MASS  $K_s$  for late-type giants

vs. supergiants or carbon stars (i.e., stars with  $(H-K)_{\text{CIT}} > 0.5$ ), since the latter two have stronger CO bandhead absorption features (which affects  $K$  much more than it does  $K_s$ ). As this may be relevant for intermediate-age star clusters whose near-IR colors are dominated by light from AGB stars, we tested the significance of this effect by using the SYNPHOT package within IRAF/STSDAS along with  $H$ - and  $K$ -band spectra of late-type giants, supergiants, and carbon stars taken by Lançon & Rocca-Volmerange (1992) and filter throughput curves taken from Cutri et al. (2003). As Fig. 11 shows, the offset between  $K$  and  $K_s$  for the different types of late-type stars only starts being significant redward of  $H-K_s \sim 0.9$ . Since the clusters in our sample all have  $H-K_s < 0.9$  (cf. Tables 5 and 6), we conclude that color term differences between supergiants and carbon stars do not significantly influence the integrated-light photometry of our clusters, and hence the cross-calibrations of Carpenter (2001) should be adequate for our purposes.

The  $K$  CIT magnitude values as well as  $(J-K)$  and  $(H-K)$  colors from Persson et al. (1983) were thus converted into the 2MASS system by using the transformation equations derived by Carpenter (2001)<sup>6</sup>. The comparison plots between  $K_s$  magnitudes and the colors for the SMC clusters in common between our work and Persson et al. are presented in Figures 12–14. The mean offsets between the  $K_s$  magnitude values from the two studies are 0.13 ( $\sigma = 0.26$ ) and 0.11 ( $\sigma = 0.44$ ) for SMC and LMC, respectively. For  $(J-K_s)$  color we calculated mean offset  $-0.08$  ( $\sigma = 0.13$ ) and  $-0.08$  ( $\sigma = 0.25$ ) for the SMC and LMC. The  $(H-K_s)$  mean offsets for the two galaxies are  $-0.06$  ( $\sigma = 0.08$ ) and  $-0.09$  ( $\sigma = 0.16$ ).

The largest differences appear in the case of NGC 152, situated in the SMC and NGC 2209 in the LMC. If we can explain the nature of these discrepancies it is plausible to assume that it is possible to explain the smaller offsets arising for the rest of the objects in the sample as well.

To investigate this in more detail we plot the  $J$ ,  $H$  and  $K_s$  frames of NGC 152 on the right side of Figure 15. The images are centered on the cluster position derived in this paper (as explained above). To simulate the measurements of Persson et al. (1983) who maximized the count rate received through their single-channel detector, we used an aperture of their size and let its center drift across a  $40'' \times 40''$  subimage located around the center position of our apertures. The step size was 1 pixel (or arcsec) and after the row or column was completed, the aperture center moved to the next one until the entire section was scanned. The measurement with the maximal flux value is assumed to be the center of that aperture in Persson et al. (1983). These simulations were done for each passband independently. The

---

<sup>6</sup>The most recent update of the transformations is available online at: <http://www.astro.caltech.edu/jmc/2mass/v3/transformations/>



results are listed in Table 7 and Table 8. For illustration purposes, we plot the apertures used in our study and the reproduction of those used by Persson et al. together in Figure 15. NGC 152 is an intermediate-age SMC cluster, and there are several bright red stars which dominate the flux in the near-infrared. (Their presence was also noted by Persson et al.) The faintness of the cluster, the bright stars and the extended nature of the cluster render the centering extremely hard for single-channel photometry. The problem is most serious for the smaller aperture, but there is a better agreement for the bigger one. The results of the comparison are shown in Table 7.

NGC 2209 is the most extreme example of differences between our study and that of Persson et al. (1983), amounting to 2.5 magnitudes in the  $K$ -band. The 2MASS images of this cluster are shown in the left three panels of Figure 15. The object is a faint cluster with an age of  $\sim 1$  Gyr. There are two bright stars dominating the flux, which are carbon stars identified as W46 and W50 by Walker (1971). Persson et al. note that they may affect the centering of their aperture and therefore likely the results of their photometry, which was performed with a single  $30''$  aperture. The offsets of the Persson’s aperture centers, reproduced by maximal flux experiments is between 10.5 and 17.5 pixels away from our position, depending on the passband used. The magnitude and color values listed in Table 2 of Persson et al. (1983) and the curves of growth from our work (presented in Figure 16) suggest that the flux of the carbon stars in NGC 2209 affects the total cluster magnitudes of Persson et al. To test our simulated position of Persson et al.’s aperture, we converted the magnitudes of Persson et al. (1983) to the 2MASS system and compared them with the corresponding values from our work after recentering our aperture on the simulated position used by Persson et al. The results are presented in Table 8. There is good agreement between  $K_s$  magnitudes and  $H - K_s$  colors,  $J - K_s$  is a little off, but there still is good agreement at the  $3\sigma$  level. The most probable reason is a slight difference in the  $J$  magnitude values. This is not surprising taking into account that the  $J$  band magnitudes could be affected by rapid variations of the water vapor content in the atmosphere. In this particular case the differences between our results and the photometry of Persson et al. are mainly caused by centering problems. We are taking into account only the photometric uncertainty and the errors of the 2MASS zero points in the analysis above. Due to the presence of several relatively bright stars in the background field and the low signal from the cluster, the errors associated with the stochastic fluctuations in the stellar background are quite high. If we take them into account, there is much better agreement between the magnitudes and colors reproduced by our experiment and the values of Persson et al. (1983).

In general, we were able to achieve agreement between our results and those of Persson et al. by assuming a center location for their measurements which is significantly off the ‘true’ center of the cluster in question. The centering discrepancies are smaller for the larger

apertures, but still large enough to alter the total magnitudes significantly.

Figure 12 is perhaps the best illustration of the effects mentioned above. The total magnitudes of the clusters in Persson et al. (1983) for the 30'' aperture compared to the data in the present paper are underestimated for 6 of 8 objects and the most probable explanation is centering of the aperture over the brightest part of the cluster population. There is an overestimate in the case of KRON 3, which is a little surprising taking into account the compact nature and the shape of the object. On the other hand a more careful inspection shows that if the aperture is placed on the geometrical center of KRON 3 it is not sampling the most luminous part of the stellar population. In general we have good agreement for the compact and bright clusters, residing in regions of relatively homogeneous foreground or Magellanic clouds stellar population (e.g. NGC419, NGC121), especially for the larger 60'' aperture. This is also the case for NGC 458, a faint cluster, measured by Persson et al. only in a single 30'' aperture. The values of  $J - K_s$  and  $H - K_s$  colors of the clusters for the smaller 30'' aperture are systematically higher in Persson et al.. The observed trend is also consistent with the expected results from the flux-maximization.

Kyeong et al. (2003) presented 2-dimensional NIR imaging of a smaller sample of 28 LMC clusters. Their observations were conducted in December 1996 with CASPIR (Cryogenic Array Spectrometer/Imager) instrument at the 2.3m telescope of the Siding Spring Observatory. The clusters were observed in the  $JHK$  passbands of the SAAO NIR system. The flux from the background fields was subtracted from the flux measured in the photometry aperture. The authors took advantage from their imaging data to determine the centers of the objects by visual inspection and used them to measure the integrated magnitudes of the clusters in 11 concentric apertures. Unfortunately the center positions were never published, so it is impossible to provide a detailed comparison between our photometry and the values in the earlier work. We transformed the values of the  $J, H$  and  $K$  total magnitudes for their largest aperture ( $D=100''$ ) into 2MASS magnitudes for the 22 objects in common, using the work of Carpenter (2001). The comparison between the datasets showed mean offsets (by means of difference between our magnitudes and the values of Kyeong et al.) :  $-0.10 \pm 0.05$ ,  $-0.06 \pm 0.04$  and  $0.00 \pm 0.03$  in  $J, H$  and  $K_S$  respectively. An inspection of the observing log published in their Table 2 revealed notes about non-photometric conditions concerning clusters observed during two of the nights. This is a possible explanation for the larger differences between our photometry and the results of Kyeong et al. in  $J$  and  $H$  bands which are much more affected by rapid changes of the atmospheric transition and water vapor content.

### 3.2. Comparison with 2MASS Extended Source Catalogue

The Extended Source Catalogue (hereafter XSC) processor in the 2MASS pipeline was designed to provide a flux measurement of the diffuse light of extended sources such as distant galaxies. As described in Jarrett et al. (2000), the XSC processor masks out point sources and substitutes the flux in the masked pixels with the surface brightness of the underlying diffuse light. When applied to star clusters in the Magellanic Clouds, one can therefore expect the XSC processor to eliminate stars that are actually genuine members of the star clusters, some of which contribute significantly to the total flux. As shown in Fig. 17, we indeed find that the XSC magnitudes (which are given for 11 concentric circular apertures) are in very good agreement with our photometry of the *unresolved* component of the clusters. However, as the *total* magnitudes of the clusters are significantly brighter than this, we discourage use of the XSC catalog for partially resolved targets such as those considered here.

## 4. Summary and Conclusions

We present a highly uniform dataset of integrated  $J$ ,  $H$  and  $K_s$  magnitudes for 75 star clusters in the Magellanic Clouds, using 2MASS survey data. There are reliable age and metallicity estimates available in the literature for the vast majority of the objects in the sample. This is the first extensive NIR survey of the clusters in these galaxies since the single-channel photometry of Persson et al. (1983). Comparing the results of their photometry with the magnitudes from our infrared array curve-of-growth measurements, we find significant differences for some objects, which we can reproduce as being due to centering problems in the early Persson et al. study.

Keeping in mind that the Persson et al. (1983) results were used to calibrate some of the most recent SSP models (Bruzual & Charlot 2003; Maraston 2005), we suggest that the photometry derived in the present work be used to calibrate and improve the existing and future SSP models in the near-IR part of the spectrum. We intend to perform a detailed comparison with the predictions of a set of simple stellar population models in a forthcoming paper, utilizing new *VRI* optical data from Goudfrooij et al. (2006).

**Acknowledgments** The authors would like to thank to the anonymous referee for the helpful suggestions and comments that improved the paper. The authors are thankful to Dennis Zaritsky and his collaborators for the kind and quick response of the inquiry about the MCPS extinction estimation tool and providing access to their online utility. This

publication makes use of data products from the Two Micron All-Sky Survey, which is a joint project of the University of Massachusetts and the Infrared Processing and Analysis Center/California Institute of Technology, funded by the National Aeronautics and Space Administration and the National Science Foundation. This research has made use of the NASA/IPAC Extragalactic Database (NED) which is operated by the Jet Propulsion Laboratory, California Institute of Technology, under contract with the National Aeronautics and Space Administration. Support for this work was provided in part by NASA through a Spitzer Space Telescope Program, through a contract issued by the Jet Propulsion Laboratory, California Institute of Technology under a contract with NASA. Support for this work was also provided in part by the STScI Director's Discretionary Research Fund.

## REFERENCES

- Alcaino, G. 1978, *A&AS*, 34, 431
- Alves, D. R., & Sarajedini, A. 1999, *ApJ*, 511, 225
- Alves, D. R. 2004, *New Astronomy Review*, 48, 659
- Beasley, M. A., Hoyle, F., & Sharples, R. M. 2002, *MNRAS*, 336, 168
- Bessell, M. S., & Brett, J. M. 1988, *PASP*, 100, 1134
- Bica, E., Claria, J. J., Dottori, H., Santos, J. F. C., & Piatti, A. E. 1996, *ApJS*, 102, 57
- Bica, E., Geisler, D., Dottori, H., Clariá, J. J., Piatti, A. E., & Santos, J. F. C. 1998, *AJ*, 116, 723
- Bruzual, A. G., & Charlot, S. 1993, *ApJ*, 405, 538
- Bruzual, G., Barbuy, B., Ortolani, S., Bica, E., Cuisinier, F., Lejeune, T., & Schiavon, R. P. 1997, *AJ*, 114, 1531
- Bruzual, G., & Charlot, S. 2003, *MNRAS*, 344, 1000
- Burstein, D., & Heiles, C. 1982, *AJ*, 87, 1165
- Carpenter, J. M. 2001, *AJ*, 121, 2851
- Casali, M. M. & Hawarden, T. G. 1992, *JCMT-UKIRT Newsletter*, No. 4, 33
- Chiosi, C., Vallenari, A., Bressan, A., Deng, L., & Ortolani, S. 1995, *A&A*, 293, 710

- Crowl, H. H., Sarajedini, A., Piatti, A. E., Geisler, D., Bica, E., Clariá, J. J., & Santos, J. F. C. 2001, *AJ*, 122, 220
- Cutri, R. M., et al. 2003, *VizieR Online Data Catalog*, 2246
- Da Costa, G. S., & Hatzidimitriou, D. 1998, *AJ*, 115, 1934
- de Grijs, R., Gilmore, G. F., Johnson, R. A., & Mackey, A. D. 2002, *MNRAS*, 331, 245
- Dirsch, B., Richtler, T., Gieren, W. P., & Hilker, M. 2000, *A&A*, 360, 133
- Ducati, J. R., Bevilacqua, C. M., Rembold, S. B., & Ribeiro, D. 2001, *ApJ*, 558, 309
- Elson, R. A., & Fall, S. M. 1988, *AJ*, 96, 1383
- Elson, R. A. W. 1991, *ApJS*, 76, 185
- Frogel, J. A., Persson, S. E., Matthews, K., & Aaronson, M. 1978, *ApJ*, 220, 75
- Frogel, J. A., Mould, J., & Blanco, V. M. 1990, *ApJ*, 352, 96
- Geisler, D., Bica, E., Dottori, H., Piatti, A. E., & Claria, J. J. 1997, *Bulletin of the American Astronomical Society*, 29, 841
- Geisler, D., Bica, E., Dottori, H., Claria, J. J., Piatti, A. E., & Santos, J. F. C. 1997, *AJ*, 114, 1920
- Goudfrooij, P., Alonso, M. V., Maraston, C., & Minniti, D. 2001, *MNRAS*, 328, 237
- Goudfrooij, P., Gilmore, D., Kissler-Patig, M., & Maraston, C., 2006, *MNRAS*, in press
- Harries, T. J., Hilditch, R. W., & Howarth, I. D. 2003, *MNRAS*, 339, 157
- Hempel, M., & Kissler-Patig, M. 2004, *A&A*, 419, 863
- Hill, V. 1999, *A&A*, 345, 430
- Hill, V., François, P., Spite, M., Primas, F., & Spite, F. 2000, *A&A*, 364, L19
- Hill, A. & Zaritsky, D. 2005, in prep
- Hodge, P., & Flower, P. 1987, *PASP*, 99, 734
- Hunter, D. A., Shaya, E. J., Holtzman, J. A., Light, R. M., O’Neil, E. J., & Lynds, R. 1995, *ApJ*, 448, 179

- Jarrett, T. H., Chester, T., Cutri, R., Schneider, S., Skrutskie, M., & Huchra, J. P. 2000, *AJ*, 119, 2498
- Jasniewicz, G., & Thevenin, F. 1994, *A&A*, 282, 717
- Johnson, R. A., Beaulieu, S. F., Gilmore, G. F., Hurley, J., Santiago, B. X., Tanvir, N. R., & Elson, R. A. W. 2001, *MNRAS*, 324, 367
- Kontizas, M., Morgan, D. H., Hatzidimitriou, D., & Kontizas, E. 1990, *A&AS*, 84, 527
- Kontizas, E., Dapergolas, A., Morgan, D. H., & Kontizas, M. 2001, *A&A*, 369, 932
- Kyeong, J.-M., Tseng, M.-J., & Byun, Y.-I. 2003, *A&A*, 409, 479
- Lançon, A., & Rocca-Volmerange, B., 1992, *A&AS*, 96, 593
- Mackey, A. D., & Gilmore, G. F. 2003, *MNRAS*, 338, 85
- Mackey, A. D., & Gilmore, G. F. 2003, *MNRAS*, 338, 120
- Maraston, C. 1998, *MNRAS*, 300, 872
- Maraston, C., Kissler-Patig, M., Brodie, J. P., Barmby, P., & Huchra, J. P. 2001, *A&A*, 370, 176
- Maraston, C. 2005, *MNRAS*, 362, 799
- Maraston, C., Greggio, L., Renzini, A., Ortolani, S., Saglia, R. P., Puzia, T. H., & Kissler-Patig, M. 2003, *A&A*, 400, 823
- Mighell, K. J., Sarajedini, A., & French, R. S. 1998, *ApJ*, 494, L189
- Nikolaev, S., Weinberg, M. D., Skrutskie, M. F., Cutri, R. M., Wheelock, S. L., Gizis, J. E.; Howard, E. M. 2000, *AJ*, 120, 3340
- Oliva, E., & Origlia, L. 1998, *A&A*, 332, 46
- Olsen, K. A. G., Hodge, P. W., Mateo, M., Olszewski, E. W., Schommer, R. A., Suntzeff, N. B., & Walker, A. R. 1998, *MNRAS*, 300, 665
- Olszewski, E. W., Schommer, R. A., Suntzeff, N. B., & Harris, H. C. 1991, *AJ*, 101, 515
- Persson, S. E., Aaronson, M., Cohen, J. G., Frogel, J. A., & Matthews, K. 1983, *ApJ*, 266, 105

- Persson, S. E., Murphy, D. C., Krzeminski, W., Roth, M., & Rieke, M. J. 1998, *AJ*, 116, 2475
- Puzia, T. H., Zepf, S. E., Kissler-Patig, M., Hilker, M., Minniti, D., & Goudfrooij, P. 2002, *A&A*, 391, 453
- Seggewiss, W., & Richtler, T. 1989, Recent Developments of Magellanic Cloud Research. A European Colloquium, held in Paris, France, May 9-11, 1989. Editors, K.S. de Boer, F. Spite, G. Stasinska; Publisher, Observatoire de Paris, Section Astrophysique de Meudon, Meudon, France, 1989. LC # QB858.5.M33 R42 1989. ISBN # NONE. P. 45, 1989, 45
- Rich, R. M., Shara, M. M., & Zurek, D. 2001, *AJ*, 122, 842
- Schlegel, D. J., Finkbeiner, D. P., & Davis, M. 1998, *ApJ*, 500, 525
- Sirianni, M., Nota, A., Leitherer, C., De Marchi, G., & Clampin, M. 2000, *ApJ*, 533, 203
- Skrutskie, M. F., et al. 1997, *ASSL Vol. 210: The Impact of Large Scale Near-IR Sky Surveys*, 25
- Stetson, P. B. 1987, *PASP*, 99, 191
- Suntzeff, N. B., Schommer, R. A., Olszewski, E. W., & Walker, A. R. 1992, *AJ*, 104, 1743
- Vazdekis, A. 1999, *ApJ*, 513, 224
- van den Bergh, S. 1981, *A&AS*, 46, 79
- Walker, M. F. 1971, *ApJ*, 167, 1
- Worthey, G. 1994, *ApJS*, 95, 107
- Zaritsky, D., Harris, J., & Thompson, I. 1997, *AJ*, 114, 1002
- Zaritsky, D. 1999, *AJ*, 118, 2824
- Zaritsky, D., Harris, J., Thompson, I. B., Grebel, E. K., & Massey, P. 2002, *AJ*, 123, 855
- Zaritsky, D., Harris, J., Thompson, I. B., & Grebel, E. K. 2004, *AJ*, 128, 1606

Table 1. SMC cluster sample.

ID	$\alpha_{2000}^a$	$\delta_{2000}^a$	Age, Errors & Ref <sup>b</sup>				[Fe/H], Err & Ref			$A_v^c$	$A_v$ err <sup>c</sup>
NGC121	00:26:49	-71:32:10	10.08	+0.05	-0.05	7	-1.71	$\pm 0.10$	7	0.18	0.02
NGC152	00:32:56	-73:06:59	9.15	+0.06	-0.07	3	-0.94	$\pm 0.15$	3	0.19	0.02
NGC176	00:35:59	-73:09:57	8.30	+0.30	-0.30	6;8	-0.6	...	8	0.24	0.03
NGC330	00:56:20	-72:27:44	7.40	+0.20	-0.40	2;4	-0.82	$\pm 0.11$	5	0.37	0.02
NGC339	00:57:45	-74:28:21	9.80	+0.08	-0.10	7	-1.50	$\pm 0.14$	7	0.18	0.02
NGC361	01:02:11	-71:36:25	9.91	+0.06	-0.07	7	-1.45	$\pm 0.11$	7	0.17	0.02
NGC411	01:07:56	-71:46:09	9.15	+0.06	-0.07	1;3	-0.68	$\pm 0.07$	1;3	0.17	0.02
NGC416	01:07:58	-72:21:25	9.84	+0.06	-0.08	7	-1.44	$\pm 0.12$	7	0.20	0.02
NGC458	01:14:54	-71:32:58	8.30	+0.18	-0.30	4	-0.23	$\pm 0.25$	4	0.23	0.02
KRON3	00:24:46	-72:47:37	9.78	+0.09	-0.11	7	-1.16	$\pm 0.09$	7	0.18	0.02
NGC419	01:08:19	-72:53:03	9.08	...	...	9	-0.6	...	9	0.32	0.02
Lindsay1	00:04:00	-73:28:00	9.89	...	...	7	-1.35	...	7	0.18	0.02
Lindsay113	01:49:30	-73:43:00	9.60	...	...	7	-1.24	...	7	0.18	0.02

<sup>a</sup>Positions  $\alpha_{2000}$  (hh:mm:ss),  $\delta_{2000}$  (dd:mm:ss) are retrieved from Simbad Astronomical Database

<sup>b</sup>The age for the clusters is given as  $\log(\text{age})$ . The CMDs of the last three objects are providing only a crude age estimation, and the errors are not given.

<sup>c</sup>The extinction information is retrieved from the website of the MCPS

References. — 1. Alves & Sarajedini (1999) 2. Chiosi et al. (1995) 3. Crowl et al. (2001) 4. Da Costa & Hatzidimitriou (1998) 5. Hill (1999) 6. Hodge & Flower (1987) 7. Mighell et al. (1998) 8. Mackey & Gilmore (2003b) 9. Seggewiss & Richtler (1989)



Table 2. LMC cluster sample.

ID	$\alpha_{2000}^a$	$\delta_{2000}^a$	Age, Errors & Ref <sup>b</sup>				[Fe/H], Err & Ref			$A_v^c$	$A_v$ err <sup>c</sup>
NGC1466	03:44:33	-71:40:18	10.10	+0.01	-0.01	5	-2.17	$\pm 0.20$	12	0.39	0.02
NGC1651	04:37:32	-70:35:06	9.30	+0.08	-0.10	5	-0.37	$\pm 0.20$	12	0.35	0.05
NGC1711	04:50:37	-69:59:06	7.70	+0.05	-0.05	2	-0.57	$\pm 0.17$	2	0.56	0.01
NGC1718	04:52:25	-67:03:06	9.30	+0.30	-0.30	4	-0.42	...	20	0.51	0.06
NGC1754	04:54:17	-70:26:30	10.19	+0.06	-0.07	11	-1.54	$\pm 0.20$	12	0.40	0.04
NGC1777	04:55:48	-74:17:00	9.08	+0.12	-0.18	5	-0.35	$\pm 0.20$	12	0.39	0.02
NGC1786	04:59:06	-67:44:42	10.18	+0.01	-0.01	5	-1.87	$\pm 0.20$	12	0.62	0.04
NGC1805	05:02:21	-66:06:42	7.00	+0.30	-0.10	1	-0.25	...	1;9	0.32	0.02
NGC1818	05:04:14	-66:26:06	7.40	+0.30	-0.10	1	-0.25	...	1;9	0.39	0.02
NGC1831	05:06:16	-64:55:06	8.50	+0.30	-0.30	4	+0.01	$\pm 0.20$	12	0.39	0.02
NGC1835	05:05:05	-69:24:12	10.22	+0.07	-0.08	11	-1.79	$\pm 0.20$	12	0.35	0.07
NGC1841	04:45:23	-83:59:48	10.09	+0.01	-0.01	5	-2.11	$\pm 0.10$	15	0.39	0.02
NGC1847	05:07:08	-68:58:18	7.42	+0.30	-0.30	4	-0.37	...	20	0.49	0.02
NGC1850	05:08:44	-68:45:36	7.50	+0.20	-0.20	3	-0.12	$\pm 0.20$	8	0.33	0.01
NGC1856	05:09:29	-69:07:36	8.12	+0.30	-0.30	4	-0.52	...	20	0.22	0.03
NGC1860	05:10:39	-68:45:12	8.28	+0.30	-0.30	4	-0.52	...	20	0.27	0.07
NGC1866	05:13:39	-65:27:54	8.12	+0.30	-0.30	4	-0.50	$\pm 0.10$	6	0.28	0.06
NGC1868	05:14:36	-63:57:18	8.74	+0.30	-0.30	4	-0.50	$\pm 0.20$	12	0.39	0.02
NGC1898	05:16:42	-69:39:24	10.15	+0.06	-0.08	11	-1.37	$\pm 0.20$	12	0.43	0.05
NGC1916	05:18:39	-69:24:24	10.20	+0.09	-0.09	20	-2.08	$\pm 0.20$	12	0.42	0.05
NGC1984	05:27:40	-69:08:06	7.06	+0.30	-0.30	4	-0.90	$\pm 0.40$	10	0.36	0.02
NGC2004	05:30:40	-67:17:12	7.30	+0.20	-0.20	3	-0.56	$\pm 0.20$	8	0.33	0.02
NGC2005	05:30:09	-69:45:06	10.22	+0.12	-0.16	11	-1.92	$\pm 0.20$	12	0.47	0.04
NGC2011	05:32:19	-67:31:18	6.99	+0.30	-0.30	4	-0.47	$\pm 0.40$	10	0.47	0.02
NGC2019	05:31:56	-70:09:36	10.25	+0.07	-0.09	11	-1.81	$\pm 0.20$	12	0.44	0.06
NGC2031	05:33:41	-70:59:12	8.20	+0.10	-0.10	2	-0.52	$\pm 0.21$	2	0.40	0.03
NGC2100	05:42:08	-69:12:42	7.20	+0.20	-0.20	3	-0.32	$\pm 0.20$	8	0.80	0.02
NGC2121	05:48:12	-71:28:48	9.51	+0.06	-0.07	13	-0.61	$\pm 0.20$	12	0.53	0.04
NGC2136	05:53:17	-69:31:42	8.00	+0.10	-0.10	2	-0.55	$\pm 0.23$	2	0.58	0.02
NGC2153	05:57:51	-66:24:00	9.11	+0.12	-0.16	5	-0.42	...	20	0.27	0.05
NGC2155	05:58:33	-65:28:36	9.51	+0.06	-0.07	13	-0.55	$\pm 0.20$	12	0.43	0.04
NGC2156	05:57:45	-68:27:36	7.60	+0.20	-0.20	3	-0.45	...	20	0.20	0.02
NGC2157	05:57:34	-69:11:48	7.60	+0.20	-0.20	3	-0.45	...	20	0.42	0.02

Table 2—Continued

ID	$\alpha_{2000}^a$	$\delta_{2000}^a$	Age, Errors & Ref <sup>b</sup>			[Fe/H], Err & Ref			$A_v^c$	$A_v$ err <sup>c</sup>	
NGC2159	05:57:57	−68:37:24	7.60	+0.20	−0.20	3	−0.45	...	20	0.29	0.03
NGC2162	06:00:31	−63:43:18	9.11	+0.12	−0.16	5	−0.23	±0.20	12	0.39	0.02
NGC2164	05:58:54	−68:31:06	7.70	+0.20	−0.20	3	−0.45	...	20	0.33	0.02
NGC2172	06:00:05	−68:38:12	7.60	+0.20	−0.20	3	−0.44	...	20	0.26	0.03
NGC2173	05:57:58	−72:58:42	9.33	+0.07	−0.09	5	−0.24	±0.20	12	0.39	0.02
NGC2193	06:06:17	−65:05:54	9.34	+0.09	−0.11	13	−0.60	±0.20	13	0.39	0.02
NGC2209	06:08:34	−73:50:30	8.98	+0.15	−0.24	5	−0.47	...	20	0.39	0.02
NGC2210	06:11:31	−69:07:18	10.20	+0.01	−0.01	5	−1.97	±0.20	12	0.39	0.02
NGC2213	06:10:42	−71:31:42	9.20	+0.10	−0.12	5	−0.01	±0.20	12	0.40	0.04
NGC2214	06:12:57	−68:15:36	7.60	+0.20	−0.20	3	−0.45	...	20	0.39	0.02
NGC2231	06:20:44	−67:31:06	9.18	+0.10	−0.13	5	−0.67	±0.20	12	0.39	0.02
NGC2249	06:25:49	−68:55:12	8.82	+0.30	−0.30	4	−0.47	...	20	0.39	0.02
NGC2257	06:30:12	−64:19:36	10.20	+0.10	−0.10	2	−1.63	±0.21	2	0.39	0.02
SL663	05:42:29	−65:21:48	9.51	+0.06	−0.07	13	−0.60	±0.20	13	0.38	0.04
SL842	06:08:15	−62:59:18	9.30	+0.08	−0.10	5	−0.36	±0.20	12	0.39	0.02
SL855	06:10:53	−65:02:36	9.13	+0.30	−0.30	4	−0.42	...	20	0.39	0.02
HODGE4	05:31:54	−64:42:00	9.34	+0.09	−0.11	13	−0.15	±0.20	12	0.39	0.02
HODGE11	06:14:22	−69:50:54	10.18	+0.01	−0.01	5	−2.06	±0.20	12	0.39	0.02
HODGE14	05:28:39	−73:37:48	9.26	+0.09	−0.11	5	−0.66	±0.20	12	0.39	0.02
R136	05:38:43	−69:06:03	6.48	+0.12	−0.18	14	−0.40	...	7;14	0.39	0.02
ESO121-003	06:03:24	−60:31:00	9.95	...	...	12;16	−0.93	...	12;16	0.39	0.02
LW431	06:13:27	−70:41:43	9.26	...	...	17	−0.85	...	17	0.39	0.02
NGC1751	04:54:12	−69:48:24	9.18	...	...	19	−0.18	...	19	0.65	0.06
NGC1783	04:59:08	−65:59:20	9.11	...	...	18	...	...	18	0.30	0.03
NGC1806	05:02:11	−67:59:20	8.70	...	...	19	−0.71	...	19	0.25	0.04
NGC1846	05:07:35	−67:27:39	9.46	...	...	19	−0.70	...	19	0.41	0.04
NGC1939	05:21:27	−69:56:59	10.04	...	...	19	−2.00	...	19	0.62	0.05
NGC1978	05:28:45	−66:14:12	9.32	...	...	18	−0.42	...	18	0.76	0.05
NGC1987	05:27:17	−70:44:06	9.40	...	...	19	−0.50	...	19	0.28	0.03
NGC2190	06:01:02	−74:43:30	9.04	...	...	19	−0.12	...	19	0.39	0.02
NGC2203	06:04:42	−75:26:20	9.26	...	...	18	−0.52	...	18	0.39	0.02

\*The notes are the same as in Table 1. The ages and metallicities for the last 11 objects are uncertain.

References. — 1. de Grijs et al. (2002) 2. Dirsch et al. (2000) 3. Elson (1991) 4. Elson & Fall (1988) 5. Geisler et al. (1997a) 6. Hill et al. (2000) 7. Hunter et al. (1995) 8. Jasniewicz & Thevenin (1994) 9. Johnson et al. (2001) 10. Oliva & Origlia (1998) 11. Olsen et al. (1998) 12. Olszewski et al. (1991) 13. Rich et al. (2001) 14. Sirianni et al. (2000) 15. Suntzeff et al. (1992) 16. Seggewiss & Richtler (1989) 17. Bica et al. (1998) 18. Geisler et al. (1997b) 19. Beasley et al. (2002) 20. Mackey & Gilmore (2003a)

Table 3. 2MASS Atlas Images of SMC clusters.

Cluster ID	N	<i>J</i>	<i>H</i>	<i>K<sub>s</sub></i>
NGC121	3	s4_aJ_asky_981020s0400256.fits	s5_aH_asky_981020s0400256.fits	s6_aK_asky_981020s0400256.fits
NGC152	3	s7_aJ_asky_980808s0580221.fits	s8_aH_asky_980808s0580221.fits	s9_aK_asky_980808s0580221.fits
NGC330	2	s4_aJ_asky_980809s0930245.fits	s5_aH_asky_980809s0930245.fits	s6_aK_asky_980809s0930245.fits
NGC339	3	s7_aJ_asky_980809s0940115.fits	s8_aH_asky_980809s0940115.fits	s9_aK_asky_980809s0940115.fits
NGC361	2	s4_aJ_asky_981021s0450256.fits	s5_aH_asky_981021s0450256.fits	s6_aK_asky_981021s0450256.fits
NGC411	3	s7_aJ_asky_981021s0560009.fits	s8_aH_asky_981021s0560009.fits	s9_aK_asky_981021s0560009.fits
NGC416	1	s1_aJ_asky_980809s1060021.fits	s2_aH_asky_980809s1060021.fits	s3_aK_asky_980809s1060021.fits
NGC419	3	s1_aJ_asky_980809s1060044.fits	s2_aH_asky_980809s1060044.fits	s3_aK_asky_980809s1060044.fits
NGC458	2	s4_aJ_asky_981021s0680021.fits	s5_aH_asky_981021s0680021.fits	s6_aK_asky_981021s0680021.fits
KRON3	2	s4_aJ_asky_980808s0470044.fits	s5_aH_asky_980808s0470044.fits	s6_aK_asky_980808s0470044.fits
LINDSAY1	3	s1_aJ_asky_980808s0210068.fits s4_aJ_asky_980808s0210080.fits	s2_aH_asky_980808s0210068.fits s5_aH_asky_980808s0210080.fits	s3_aK_asky_980808s0210068.fits s6_aK_asky_980808s0210080.fits
LINDSAY113	4	s7_aJ_asky_981008s0590186.fits	s8_aH_asky_981008s0590186.fits	s9_aK_asky_981008s0590186.fits

Table 4. 2MASS Atlas Images of LMC clusters.

Cluster ID	N	<i>J</i>	<i>H</i>	<i>K<sub>s</sub></i>
NGC1466	2	s1_aJ_asky_981027s0940021.fits	s2_aH_asky_981027s0940021.fits	s3_aK_asky_981027s0940021.fits
NGC1651	2	s1_aJ_asky_991026s1140068.fits	s2_aH_asky_991026s1140068.fits	s3_aK_asky_991026s1140068.fits
NGC1711	2	s1_aJ_asky_980401s0140186.fits	s2_aH_asky_980401s0140186.fits	s3_aK_asky_980401s0140186.fits
NGC1718	1	s1_aJ_asky_981025s0810056.fits	s2_aH_asky_981025s0810056.fits	s3_aK_asky_981025s0810056.fits
NGC1754	3	s1_aJ_asky_981025s0820068.fits	s2_aH_asky_981025s0820068.fits	s3_aK_asky_981025s0820068.fits
NGC1777	3	s1_aJ_asky_981202s0710162.fits	s2_aH_asky_981202s0710162.fits	s3_aK_asky_981202s0710162.fits
NGC1786	3	s1_aJ_asky_981025s0860186.fits	s2_aH_asky_981025s0860186.fits	s3_aK_asky_981025s0860186.fits
NGC1805	2	s1_aJ_asky_981025s0950009.fits	s2_aH_asky_981025s0950009.fits	s3_aK_asky_981025s0950009.fits
NGC1818	2	s4_aJ_asky_981025s0970033.fits	s5_aH_asky_981025s0970033.fits	s6_aK_asky_981025s0970033.fits
NGC1831	3	s1_aJ_asky_990129s0150221.fits	s2_aH_asky_990129s0150221.fits	s3_aK_asky_990129s0150221.fits
NGC1835	2	s4_aJ_asky_981025s0980115.fits	s5_aH_asky_981025s0980115.fits	s6_aK_asky_981025s0980115.fits
NGC1841	5	s4_aJ_asky_000221s0250009.fits	s5_aH_asky_000221s0250009.fits	s6_aK_asky_000221s0250009.fits
NGC1847	2	s4_aJ_asky_981026s0820139.fits	s5_aH_asky_981026s0820139.fits	s6_aK_asky_981026s0820139.fits
NGC1850	3	s7_aJ_asky_981026s0830127.fits	s8_aH_asky_981026s0830127.fits	s9_aK_asky_981026s0830127.fits
NGC1856	2	s1_aJ_asky_981026s0830150.fits	s2_aH_asky_981026s0830150.fits	s3_aK_asky_981026s0830150.fits
NGC1860	3	s1_aJ_asky_981026s0840139.fits	s2_aH_asky_981026s0840139.fits	s3_aK_asky_981026s0840139.fits
NGC1866	1	s1_aJ_asky_981210s0290245.fits	s2_aH_asky_981210s0290245.fits	s3_aK_asky_981210s0290245.fits
NGC1868	1	s1_aJ_asky_000218s0270092.fits	s2_aH_asky_000218s0270092.fits	s3_aK_asky_000218s0270092.fits
NGC1898	3	s4_aJ_asky_981220s0810174.fits	s5_aH_asky_981220s0810174.fits	s6_aK_asky_981220s0810174.fits
NGC1916	2	s4_aJ_asky_981220s0830162.fits	s5_aH_asky_981220s0830162.fits	s6_aK_asky_981220s0830162.fits
NGC1984	2	s1_aJ_asky_000209s0340150.fits	s2_aH_asky_000209s0340150.fits	s3_aK_asky_000209s0340150.fits
NGC2004	1	s1_aJ_asky_000228s0210068.fits	s2_aH_asky_000228s0210068.fits	s3_aK_asky_000228s0210068.fits
NGC2005	2	s1_aJ_asky_000228s0210174.fits	s2_aH_asky_000228s0210174.fits	s3_aK_asky_000228s0210174.fits
NGC2011	2	s4_aJ_asky_000327s0270198.fits	s5_aH_asky_000327s0270198.fits	s6_aK_asky_000327s0270198.fits
NGC2019	1	s1_aJ_asky_000327s0270080.fits	s2_aH_asky_000327s0270080.fits	s3_aK_asky_000327s0270080.fits
NGC2031	3	s1_aJ_asky_000206s0210044.fits	s2_aH_asky_000206s0210044.fits	s3_aK_asky_000206s0210044.fits
NGC2100	2	s4_aJ_asky_980321s0070127.fits	s5_aH_asky_980321s0070127.fits	s6_aK_asky_980321s0070127.fits
NGC2121	3	s7_aJ_asky_980321s0120245.fits	s8_aH_asky_980321s0120245.fits	s9_aK_asky_980321s0120245.fits
NGC2136	2	s4_aJ_asky_981025s1070162.fits	s5_aH_asky_981025s1070162.fits	s6_aK_asky_981025s1070162.fits
NGC2153	3	s7_aJ_asky_981025s1110033.fits	s8_aH_asky_981025s1110033.fits	s9_aK_asky_981025s1110033.fits
NGC2155	3	s1_aJ_asky_981212s0540245.fits	s2_aH_asky_981212s0540245.fits	s3_aK_asky_981212s0540245.fits
NGC2156	2	s4_aJ_asky_981025s1110115.fits	s5_aH_asky_981025s1110115.fits	s6_aK_asky_981025s1110115.fits
NGC2157	2	s1_aJ_asky_981025s1110150.fits	s2_aH_asky_981025s1110150.fits	s3_aK_asky_981025s1110150.fits
NGC2159	1	s1_aJ_asky_981025s1110127.fits	s2_aH_asky_981025s1110127.fits	s3_aK_asky_981025s1110127.fits
NGC2162	2	s1_aJ_asky_981212s0560174.fits	s2_aH_asky_981212s0560174.fits	s3_aK_asky_981212s0560174.fits

Table 4—Continued

Cluster ID	N	<i>J</i>	<i>H</i>	<i>K<sub>s</sub></i>
NGC2164	3	s4_aJ_asky_981025s1120150.fits	s5_aH_asky_981025s1120150.fits	s6_aK_asky_981025s1120150.fits
NGC2172	2	s4_aJ_asky_981026s1010127.fits	s5_aH_asky_981026s1010127.fits	s6_aK_asky_981026s1010127.fits
NGC2173	2	s4_aJ_asky_981204s0690056.fits	s5_aH_asky_981204s0690056.fits	s6_aK_asky_981204s0690056.fits
NGC2193	2	s1_aJ_asky_981212s0680233.fits	s2_aH_asky_981212s0680233.fits	s3_aK_asky_981212s0680233.fits
NGC2209	2	s4_aJ_asky_981204s0820186.fits	s5_aH_asky_981204s0820186.fits	s6_aK_asky_981204s0820186.fits
NGC2210	2	s1_aJ_asky_981026s1220127.fits	s2_aH_asky_981026s1220127.fits	s3_aK_asky_981026s1220127.fits
NGC2213	3	s7_aJ_asky_981026s1220021.fits	s8_aH_asky_981026s1220021.fits	s9_aK_asky_981026s1220021.fits
NGC2214	3	s1_aJ_asky_981026s1230103.fits	s2_aH_asky_981026s1230103.fits	s3_aK_asky_981026s1230103.fits
NGC2231	1	s1_aJ_asky_981208s0760080.fits	s2_aH_asky_981208s0760080.fits	s3_aK_asky_981208s0760080.fits
NGC2249	2	s1_aJ_asky_981208s0800139.fits	s2_aH_asky_981208s0800139.fits	s3_aK_asky_981208s0800139.fits
NGC2257	2	s4_aJ_asky_981212s1110080.fits	s5_aH_asky_981212s1110080.fits	s6_aK_asky_981212s1110080.fits
SL663	2	s1_aJ_asky_981210s0820033.fits	s2_aH_asky_981210s0820033.fits	s3_aK_asky_981210s0820033.fits
SL842	2	s1_aJ_asky_981212s0700139.fits	s2_aH_asky_981212s0700139.fits	s3_aK_asky_981212s0700139.fits
SL855	1	s1_aJ_asky_981212s0730044.fits	s2_aH_asky_981212s0730044.fits	s3_aK_asky_981212s0730044.fits
HODGE4	3	s7_aJ_asky_981210s0600056.fits	s8_aH_asky_981210s0600056.fits	s9_aK_asky_981210s0600056.fits
HODGE11	3	s7_aJ_asky_981026s1240174.fits	s8_aH_asky_981026s1240174.fits	s9_aK_asky_981026s1240174.fits
HODGE14	2	s4_aJ_asky_981202s1100080.fits	s5_aH_asky_981202s1100080.fits	s6_aK_asky_981202s1100080.fits
ESO121-003	1	s1_aJ_asky_981212s0580033.fits	s2_aH_asky_981212s0580033.fits	s3_aK_asky_981212s0580033.fits
LW431	3	s7_aJ_asky_981026s1240056.fits	s8_aH_asky_981026s1240056.fits	s9_aK_asky_981026s1240056.fits
NGC1751	2	s1_aJ_asky_981025s0820103.fits	s2_aH_asky_981025s0820103.fits	s3_aK_asky_981025s0820103.fits
NGC1783	3	s7_aJ_asky_981029s0370009.fits	s8_aH_asky_981029s0370009.fits	s9_aK_asky_981029s0370009.fits
NGC1806	2	s1_aJ_asky_981025s0950092.fits	s2_aH_asky_981025s0950092.fits	s3_aK_asky_981025s0950092.fits
NGC1846	3	s7_aJ_asky_981026s0820198.fits	s8_aH_asky_981026s0820198.fits	s9_aK_asky_981026s0820198.fits
NGC1939	2	s1_aJ_asky_981220s0850186.fits	s2_aH_asky_981220s0850186.fits	s3_aK_asky_981220s0850186.fits
NGC1978	2	s1_aJ_asky_000212s0190021.fits	s2_aH_asky_000212s0190021.fits	s3_aK_asky_000212s0190021.fits
NGC1987	3	s4_aJ_asky_000209s0340221.fits	s5_aH_asky_000209s0340221.fits	s6_aK_asky_000209s0340221.fits
NGC2190	2	s4_aJ_asky_981204s0710127.fits	s5_aH_asky_981204s0710127.fits	s6_aK_asky_981204s0710127.fits
NGC2203	2	s1_aJ_asky_981204s0730162.fits	s2_aH_asky_981204s0730162.fits	s3_aK_asky_981204s0730162.fits

Table 5. Photometry of SMC clusters.

Cluster ID	$\alpha_{2000}$	$\delta_{2000}$	$d''$	Flag	$R''$	$J$	$J_{err}$	$H$	$H_{err}$	$K$	$K_{err}$
LINDSAY1	00:03:55.2	-73:28:12.4	16.5	BBB	20	14.63	0.06	14.37	0.12	14.97	0.27
					40	12.60	0.03	12.23	0.04	12.27	0.05
					60	11.67	0.03	11.29	0.03	11.17	0.04
					80	10.88	0.02	10.42	0.03	10.30	0.03
					100	10.52	0.03	10.04	0.03	9.97	0.03
					120	10.35	0.03	9.87	0.03	9.82	0.03
					140	10.25	0.04	9.79	0.04	9.73	0.04
					160	10.09	0.04	9.61	0.04	9.57	0.04
					180	9.92	0.04	9.40	0.04	9.37	0.05
					200	9.83	0.05	9.31	0.05	9.30	0.05
KRON3	00:24:42.1	-72:47:35.2	17	AAA	20	12.04	0.02	11.91	0.01	11.92	0.02
					40	10.90	0.01	10.36	0.01	10.24	0.01
					60	10.34	0.01	9.88	0.01	9.70	0.01
					80	10.00	0.01	9.57	0.01	9.41	0.01
					100	9.79	0.02	9.38	0.01	9.23	0.01
					120	9.60	0.02	9.19	0.01	9.05	0.01
					140	9.44	0.02	9.05	0.01	8.89	0.02
					160	9.38	0.02	9.03	0.01	8.86	0.02
NGC121	00:26:48.4	-71:32:08.3	3.5	AAB	20	10.63	0.01	9.95	0.01	9.81	0.01
					40	9.84	0.01	9.20	0.01	9.07	0.01
					60	9.54	0.01	8.92	0.01	8.83	0.01
					80	9.37	0.01	8.77	0.01	8.67	0.01
					100	9.23	0.01	8.65	0.01	8.58	0.01
					120	9.19	0.02	8.62	0.01	8.55	0.01
					140	9.16	0.02	8.61	0.02	8.53	0.02
					160	9.12	0.02	8.57	0.02	8.50	0.02
					180	9.07	0.03	8.53	0.02	8.47	0.02
					200	9.04	0.03	8.51	0.03	8.45	0.03
NGC152	00:32:54.4	-73:06:54.1	8.5	AAA	20	13.63	0.03	13.63	0.04	13.22	0.04
					40	11.65	0.02	10.95	0.01	10.62	0.01
					60	10.81	0.02	10.01	0.01	9.67	0.01
					80	10.51	0.02	9.68	0.01	9.35	0.01

Table 5—Continued

Cluster ID	$\alpha_{2000}$	$\delta_{2000}$	$d''$	Flag	$R''$	$J$	$J_{err}$	$H$	$H_{err}$	$K$	$K_{err}$
					100	10.31	0.02	9.51	0.02	9.17	0.01
					120	10.23	0.03	9.46	0.02	9.12	0.02
					140	10.16	0.03	9.41	0.03	9.08	0.02
					160	10.07	0.04	9.32	0.03	9.03	0.03
					180	9.97	0.04	9.27	0.04	8.98	0.03
					200	9.94	0.05	9.23	0.04	8.97	0.04
NGC330	00:56:18.0	-72:27:46.4	9.5	AAA	20	9.66	0.01	9.19	0.01	9.10	0.01
					40	8.70	0.01	8.17	0.01	8.03	0.01
					60	8.34	0.01	7.79	0.01	7.62	0.01
					80	8.31	0.01	7.77	0.01	7.60	0.01
					100	8.12	0.01	7.54	0.01	7.33	0.01
					120	8.06	0.02	7.51	0.02	7.31	0.02
					140	8.03	0.02	7.49	0.02	7.30	0.02
					160	7.99	0.03	7.44	0.03	7.25	0.03
					180	7.94	0.03	7.39	0.03	7.23	0.04
					200	7.91	0.04	7.38	0.04	7.21	0.04
NGC339	00:57:45.2	-74:28:14.3	7	AAB	20	13.08	0.02	12.49	0.02	12.33	0.02
					40	11.82	0.02	11.23	0.02	11.06	0.02
					60	11.10	0.02	10.74	0.02	10.45	0.02
					80	10.72	0.02	10.30	0.02	10.15	0.02
					100	10.52	0.03	10.16	0.03	9.96	0.03
					120	10.35	0.03	10.08	0.04	9.83	0.03
					140	10.22	0.04	10.02	0.05	9.72	0.04
					160	10.15	0.04	10.02	0.06	9.69	0.05
					180	10.06	0.05	9.91	0.07	9.56	0.06
NGC361	01:02:10.8	-71:36:19.3	5	AAA	20	12.68	0.02	11.20	0.01	11.09	0.01
					40	11.45	0.02	10.51	0.01	10.39	0.01
					60	10.80	0.02	10.02	0.01	9.87	0.02
					80	10.48	0.02	9.71	0.02	9.62	0.02
					100	10.30	0.03	9.55	0.02	9.42	0.02
					120	10.18	0.03	9.46	0.02	9.21	0.03
					140	10.06	0.04	9.37	0.03	9.16	0.04



Table 5—Continued

Cluster ID	$\alpha_{2000}$	$\delta_{2000}$	$d''$	Flag	$R''$	$J$	$J_{err}$	$H$	$H_{err}$	$K$	$K_{err}$
					160	9.97	0.05	9.29	0.04	9.15	0.05
					180	9.92	0.06	9.24	0.04	9.11	0.06
					200	9.87	0.07	9.21	0.05	9.10	0.07
NGC411	01:07:54.4	-71:46:01.4	10.5	AAA	20	12.26	0.02	11.69	0.02	11.44	0.02
					40	10.90	0.02	10.16	0.02	9.82	0.01
					60	10.53	0.03	9.86	0.03	9.65	0.02
					80	10.26	0.04	9.72	0.04	9.47	0.04
					100	10.14	0.05	9.58	0.06	9.36	0.05
					120	10.09	0.07	9.50	0.07	9.29	0.07
					140	10.01	0.09	9.40	0.09	9.21	0.09
					160	9.96	0.11	9.35	0.12	9.20	0.11
					180	9.88	0.13	9.26	0.14	9.12	0.13
					200	9.86	0.16	9.21	0.16	9.09	0.16
NGC416	01:07:58.8	-72:21:18.6	7	AAA	20	10.80	0.01	10.28	0.01	10.35	0.01
					40	10.08	0.01	9.47	0.01	9.42	0.01
					60	9.79	0.01	9.18	0.01	9.09	0.01
					80	9.66	0.02	9.03	0.01	8.95	0.01
					100	9.60	0.02	8.95	0.02	8.86	0.02
					120	9.53	0.02	8.89	0.02	8.78	0.03
					140	9.44	0.03	8.80	0.03	8.71	0.03
					160	9.40	0.03	8.76	0.04	8.69	0.04
					180	9.34	0.04	8.69	0.04	8.61	0.05
					200	9.29	0.05	8.62	0.05	8.58	0.06
NGC419	01:08:18.0	-72:52:60.0	4	BBB	20	10.05	0.01	9.32	0.01	9.01	0.01
					40	9.15	0.01	8.43	0.01	8.09	0.01
					60	8.76	0.01	8.06	0.01	7.69	0.01
					80	8.50	0.01	7.80	0.01	7.43	0.01
					100	8.41	0.02	7.70	0.01	7.36	0.01
					120	8.36	0.02	7.64	0.01	7.32	0.01
					140	8.31	0.02	7.60	0.02	7.28	0.02
					160	8.27	0.03	7.55	0.02	7.22	0.02
					180	8.24	0.04	7.53	0.03	7.19	0.03

Table 5—Continued

Cluster ID	$\alpha_{2000}$	$\delta_{2000}$	$d''$	Flag	$R''$	$J$	$J_{err}$	$H$	$H_{err}$	$K$	$K_{err}$
					200	8.19	0.04	7.47	0.03	7.13	0.03
NGC458	01:14:53.1	-71:33:00.3	5	AAB	20	12.27	0.01	11.92	0.01	11.85	0.02
					40	11.38	0.01	11.12	0.01	10.99	0.02
					60	11.01	0.01	10.80	0.01	10.64	0.02
					80	10.81	0.02	10.69	0.02	10.50	0.02
					100	10.70	0.02	10.77	0.03	10.43	0.03
					120	10.64	0.02	10.87	0.04	10.42	0.04
					140	10.60	0.03	11.05	0.06	10.49	0.05
					160	10.56	0.03	11.12	0.08	10.37	0.06
					180	10.54	0.04	11.62	0.17	10.44	0.08
LINDSAY113	01:49:25.8	-73:43:32.3	36.5	BBA	20	14.43	0.04	13.45	0.04	13.90	0.08
					40	12.88	0.03	11.87	0.02	12.13	0.04
					60	11.52	0.02	10.54	0.01	10.36	0.01
					80	11.09	0.02	10.07	0.01	9.99	0.02
					100	10.62	0.02	9.57	0.01	9.51	0.01
					120	10.51	0.03	9.39	0.02	9.41	0.02
					130	10.47	0.03	9.31	0.02	9.35	0.02

–Column 1 is the cluster designation, 2 and 3 are the right ascension and declination of the position used to center the apertures for the integral photometry. Column 4 is the offset of that position with respect of the cluster coordinates in SIMBAD, measured on 2MASS atlas images. Column 5 contains a flag, providing information about the age (first letter), metallicity estimates (second letter) and the photometry (third letter) for each cluster. A is corresponding to a reliable age, metallicity and photometry, B denotes the cases when the age and metallicity values are uncertain and when used in the third position B stands for the cases described in Section 2.7 or if the photometry was provided in aperture sizes smaller than 200". The radii of the apertures used for each measurement are listed in column 6. The photometry information is given in columns 7 – 12, in the order:  $J$  magnitude, error of photometry in  $J$ , and the same information for the other two survey bands  $H$  and  $K_s$ . The error of photometry in each band is calculated as a square root of the quadrature sum of the zero point error, internal error of the photometry, and the error due to stochastic fluctuations of the background stellar population.

Table 6. Photometry of LMC clusters.

Cluster ID	$\alpha_{2000}$	$\delta_{2000}$	$d''$	Flag	$R''$	$J$	$J_{err}$	$H$	$H_{err}$	$K$	$K_{err}$
NGC1466	03:44:32.8	-71:40:16.6	2.5	AAA	20	10.94	0.01	10.44	0.01	10.35	0.01
					40	10.17	0.01	9.70	0.01	9.60	0.01
					60	9.83	0.02	9.39	0.01	9.30	0.01
					80	9.67	0.02	9.23	0.01	9.12	0.02
					100	9.58	0.03	9.15	0.02	9.03	0.02
					120	9.55	0.04	9.12	0.03	9.00	0.03
					140	9.52	0.05	9.08	0.03	8.95	0.04
					160	9.48	0.07	9.06	0.04	8.91	0.05
					180	9.45	0.08	9.03	0.05	8.88	0.06
					200	9.44	0.10	9.02	0.07	8.87	0.08
NGC1651	04:37:33.2	-70:35:20.0	15.5	AAA	20	12.98	0.02	12.55	0.02	12.34	0.03
					40	11.64	0.02	11.06	0.02	11.09	0.03
					60	11.10	0.02	10.49	0.02	10.43	0.03
					80	10.23	0.02	9.46	0.02	9.25	0.02
					100	10.00	0.02	9.23	0.02	9.10	0.02
					120	9.92	0.03	9.13	0.02	9.03	0.03
					140	9.78	0.04	9.01	0.03	8.86	0.03
					160	9.72	0.05	8.91	0.04	8.77	0.04
					180	9.71	0.06	8.88	0.04	8.73	0.05
					200	9.69	0.07	8.85	0.05	8.72	0.06
NGC1841	04:45:22.6	-83:59:53.1	6	AAB	20	12.59	0.02	12.07	0.02	11.88	0.02
					40	11.40	0.02	10.82	0.02	10.69	0.02
					60	10.64	0.02	10.09	0.02	9.99	0.02
					80	10.26	0.03	9.68	0.03	9.62	0.03
					100	9.97	0.03	9.36	0.03	9.33	0.04
					120	9.75	0.04	9.12	0.04	9.06	0.04
NGC1711	04:50:36.8	-69:58:58.9	6	AAA	20	10.28	0.01	9.53	0.01	9.52	0.01
					40	9.50	0.01	8.96	0.01	9.02	0.01
					60	9.36	0.01	8.88	0.01	8.93	0.02
					80	9.07	0.02	8.58	0.02	8.69	0.02
					100	8.97	0.02	8.50	0.02	8.59	0.03

Table 6—Continued

Cluster ID	$\alpha_{2000}$	$\delta_{2000}$	$d''$	Flag	$R''$	$J$	$Jerr$	$H$	$Herr$	$K$	$Kerr$
					120	8.89	0.03	8.44	0.03	8.51	0.04
					140	8.81	0.03	8.34	0.04	8.40	0.05
					160	8.74	0.04	8.27	0.05	8.32	0.06
					180	8.70	0.05	8.20	0.06	8.25	0.08
					200	8.60	0.05	8.16	0.07	8.13	0.09
NGC1718	04:52:27.1	-67:03:02.0	13.5	ABA	20	11.43	0.01	11.12	0.01	10.43	0.01
					40	10.39	0.01	9.70	0.01	9.53	0.01
					60	10.07	0.01	9.21	0.01	9.04	0.01
					80	9.80	0.01	8.93	0.01	8.63	0.01
					100	9.71	0.02	8.85	0.01	8.58	0.01
					120	9.66	0.02	8.82	0.01	8.55	0.02
					140	9.57	0.02	8.77	0.02	8.49	0.02
					160	9.33	0.02	8.52	0.02	8.24	0.02
					180	9.12	0.03	8.32	0.02	8.01	0.02
					200	9.06	0.03	8.30	0.02	7.92	0.03
NGC1751	04:54:11.4	-69:48:33.1	10.5	BBA	20	11.63	0.01	10.79	0.01	10.27	0.01
					40	10.16	0.01	9.25	0.01	8.81	0.01
					60	9.88	0.02	8.84	0.01	8.41	0.01
					80	9.66	0.02	8.68	0.02	8.30	0.02
					100	9.52	0.03	8.60	0.02	8.23	0.02
					120	9.45	0.04	8.56	0.03	8.19	0.03
					140	9.39	0.05	8.52	0.04	8.17	0.04
					160	9.28	0.06	8.42	0.05	8.08	0.05
					180	9.24	0.07	8.40	0.07	8.05	0.06
					200	9.19	0.08	8.37	0.08	8.03	0.07
NGC1754	04:54:18.4	-70:26:29.1	8	AAB	20	10.78	0.01	10.23	0.01	10.21	0.01
					40	10.21	0.02	9.70	0.01	9.57	0.02
					60	9.99	0.03	9.41	0.02	9.33	0.02
					80	9.86	0.04	9.33	0.03	9.18	0.04
					100	9.74	0.06	9.24	0.04	9.08	0.05
					120	9.66	0.08	9.16	0.06	9.04	0.07
					140	9.63	0.10	9.13	0.07	9.01	0.10

Table 6—Continued

Cluster ID	$\alpha_{2000}$	$\delta_{2000}$	$d''$	Flag	$R''$	$J$	$Jerr$	$H$	$Herr$	$K$	$Kerr$
					160	9.60	0.13	9.10	0.10	8.98	0.12
NGC1777	04:55:51.3	-74:16:59.3	14	AAA	20	11.21	0.01	10.74	0.01	10.60	0.01
					40	9.05	0.01	8.57	0.01	8.44	0.01
					60	8.65	0.01	8.24	0.01	8.12	0.01
					80	8.60	0.01	8.19	0.01	8.07	0.01
					100	8.55	0.01	8.15	0.01	8.05	0.02
					120	8.53	0.01	8.13	0.02	8.03	0.02
					140	8.52	0.01	8.11	0.03	8.03	0.03
					160	8.51	0.01	8.10	0.03	8.02	0.03
					180	8.50	0.01	8.09	0.04	8.01	0.04
					200	8.48	0.01	8.07	0.05	8.01	0.05
NGC1786	04:59:07.3	-67:44:40.9	8	AAB	20	9.08	0.01	8.63	0.01	8.54	0.01
					40	8.71	0.01	8.24	0.01	8.14	0.01
					60	8.57	0.01	8.09	0.01	8.00	0.01
					80	8.51	0.01	8.03	0.01	7.94	0.01
					98	8.48	0.01	7.99	0.01	7.91	0.01
NGC1783	04:59:08.8	-65:59:12.8	8	BBB	20	10.83	0.01	10.13	0.01	10.06	0.01
					40	9.69	0.01	9.04	0.01	8.93	0.01
					60	9.23	0.01	8.62	0.01	8.52	0.01
					80	8.90	0.01	8.26	0.01	8.17	0.01
					100	8.69	0.01	8.05	0.01	7.95	0.01
					120	8.46	0.02	7.78	0.01	7.64	0.01
					134	8.40	0.02	7.70	0.02	7.53	0.02
NGC1806	05:02:12.4	-67:59:09.1	14	BBA	20	10.31	0.01	9.84	0.01	9.19	0.01
					40	9.67	0.01	9.16	0.01	8.73	0.01
					60	9.19	0.01	8.62	0.01	8.21	0.01
					80	8.95	0.01	8.33	0.01	7.97	0.01
					100	8.85	0.01	8.24	0.01	7.89	0.01
					120	8.77	0.02	8.17	0.01	7.82	0.01
					140	8.70	0.02	8.12	0.02	7.78	0.02
					160	8.65	0.02	8.05	0.02	7.73	0.02
					180	8.55	0.02	7.91	0.02	7.59	0.02

Table 6—Continued

Cluster ID	$\alpha_{2000}$	$\delta_{2000}$	$d''$	Flag	$R''$	$J$	$J_{err}$	$H$	$H_{err}$	$K$	$K_{err}$
					200	8.52	0.03	7.90	0.03	7.57	0.02
NGC1805	05:02:20.8	-66:06:41.1	0	ABB	20	8.73	0.01	8.02	0.01	7.66	0.01
					40	8.63	0.01	7.96	0.01	7.61	0.01
					60	8.55	0.01	7.91	0.01	7.57	0.01
					80	8.50	0.01	7.87	0.01	7.53	0.01
					100	8.49	0.01	7.87	0.01	7.52	0.01
					120	8.47	0.01	7.86	0.01	7.52	0.02
					140	8.46	0.01	7.86	0.02	7.51	0.02
					150	8.43	0.01	7.84	0.02	7.50	0.02
NGC1818	05:04:13.8	-66:26:04.4	1	ABA	20	9.38	0.01	8.71	0.01	8.52	0.01
					40	8.51	0.01	7.91	0.01	8.05	0.01
					60	8.31	0.01	7.66	0.01	7.77	0.01
					80	8.26	0.01	7.63	0.01	7.74	0.01
					100	8.19	0.01	7.62	0.01	7.72	0.01
					120	8.05	0.01	7.46	0.01	7.53	0.01
					140	8.03	0.01	7.44	0.01	7.49	0.01
					160	7.98	0.01	7.37	0.01	7.40	0.01
					180	7.96	0.01	7.36	0.01	7.40	0.01
					200	7.95	0.01	7.35	0.01	7.39	0.01
NGC1835	05:05:06.3	-69:24:13.1	7	AAB	20	6.85	0.01	6.39	0.01	6.26	0.01
					40	6.36	0.01	5.89	0.01	5.77	0.01
					60	6.18	0.01	5.66	0.01	5.54	0.01
					80	6.05	0.01	5.54	0.01	5.44	0.02
					100	5.99	0.02	5.48	0.02	5.40	0.02
					120	5.94	0.02	5.44	0.03	5.35	0.03
					130	5.92	0.03	5.41	0.03	5.33	0.04
NGC1831	05:06:15.9	-64:55:05.2	0	AAA	20	11.78	0.01	11.51	0.01	11.46	0.01
					40	10.56	0.01	10.22	0.01	10.34	0.01
					60	9.86	0.01	9.34	0.01	9.15	0.01
					80	9.65	0.02	9.10	0.02	8.92	0.01
					100	9.50	0.02	8.96	0.02	8.81	0.02
					120	9.40	0.03	8.90	0.03	8.73	0.02

Table 6—Continued

Cluster ID	$\alpha_{2000}$	$\delta_{2000}$	$d''$	Flag	$R''$	$J$	$Jerr$	$H$	$Herr$	$K$	$Kerr$
					140	9.28	0.03	8.85	0.03	8.59	0.03
					160	9.17	0.04	8.72	0.04	8.50	0.03
					180	9.11	0.05	8.66	0.05	8.44	0.04
					200	9.08	0.06	8.64	0.06	8.43	0.05
NCC1847	05:07:07.5	-68:58:22.1	5	ABA	20	10.53	0.01	10.19	0.01	9.93	0.01
					40	10.02	0.01	9.45	0.01	9.40	0.01
					60	9.82	0.02	9.36	0.02	9.30	0.03
					80	9.68	0.02	9.23	0.03	9.17	0.04
					100	9.55	0.03	9.07	0.04	9.01	0.05
					120	9.44	0.04	9.05	0.05	8.87	0.07
					140	9.38	0.05	9.01	0.07	8.81	0.09
					160	9.30	0.06	8.94	0.09	8.69	0.11
					180	9.25	0.08	8.91	0.11	8.65	0.13
					200	9.13	0.09	8.68	0.11	8.40	0.13
NGC1846	05:07:34.9	-67:27:45.5	7	BBB	20	11.03	0.01	10.35	0.01	10.10	0.01
					40	9.85	0.01	9.13	0.01	8.79	0.01
					60	9.18	0.01	8.42	0.01	8.07	0.01
					80	8.82	0.02	8.08	0.01	7.76	0.01
					100	8.59	0.02	7.85	0.01	7.51	0.01
					120	8.42	0.02	7.66	0.02	7.30	0.02
					140	8.36	0.03	7.63	0.02	7.26	0.02
					160	8.30	0.03	7.58	0.03	7.21	0.03
NGC1850	05:08:45.4	-68:45:41.5	10.5	AAB	20	9.81	0.01	9.51	0.01	9.30	0.01
					40	8.79	0.01	8.40	0.01	8.26	0.01
					60	8.27	0.01	7.85	0.01	7.71	0.01
					80	8.01	0.01	7.57	0.02	7.42	0.02
					100	7.88	0.02	7.39	0.02	7.30	0.02
					120	7.74	0.02	7.26	0.02	7.16	0.02
					140	7.66	0.02	7.16	0.03	7.05	0.03
					160	7.53	0.03	7.01	0.03	6.89	0.03
NGC1856	05:09:29.8	-69:07:40.7	6.5	ABA	20	10.19	0.01	9.90	0.01	9.60	0.01
					40	9.33	0.01	8.93	0.01	8.80	0.01

Table 6—Continued

Cluster ID	$\alpha_{2000}$	$\delta_{2000}$	$d''$	Flag	$R''$	$J$	$J_{err}$	$H$	$H_{err}$	$K$	$K_{err}$
					60	8.98	0.02	8.59	0.02	8.44	0.02
					80	8.76	0.02	8.33	0.03	8.14	0.03
					100	8.57	0.03	8.12	0.03	7.94	0.03
					120	8.46	0.04	7.99	0.04	7.83	0.05
					140	8.40	0.05	7.92	0.05	7.78	0.06
					160	8.26	0.06	7.74	0.06	7.61	0.07
					180	8.17	0.07	7.69	0.07	7.54	0.08
					200	8.06	0.07	7.58	0.08	7.49	0.10
NGC1860	05:10:38.8	-68:45:11.0	0	ABB	20	13.49	0.07	13.23	0.10	13.68	0.18
					40	12.66	0.12	12.54	0.19	12.49	0.21
					60	12.21	0.18	12.36	0.36	11.98	0.30
					80	11.62	0.18	11.40	0.26	11.57	0.37
					100	11.06	0.17	10.46	0.17	10.57	0.22
					120	11.01	0.24	10.30	0.21	10.47	0.30
NGC1866	05:13:38.5	-65:27:51.3	2.5	AAA	20	10.11	0.01	9.63	0.01	9.50	0.01
					40	9.05	0.01	8.59	0.01	8.41	0.01
					60	8.72	0.01	8.28	0.01	8.11	0.01
					80	8.48	0.02	8.03	0.01	7.87	0.01
					100	8.23	0.02	7.72	0.01	7.51	0.01
					120	8.16	0.02	7.66	0.02	7.45	0.02
					140	8.10	0.03	7.58	0.02	7.38	0.02
					160	8.07	0.04	7.56	0.03	7.36	0.03
					180	8.04	0.04	7.53	0.03	7.33	0.03
					200	8.01	0.05	7.51	0.04	7.29	0.04
NGC1868	05:14:35.8	-63:57:14.3	4.5	AAA	20	11.01	0.01	10.47	0.01	10.39	0.01
					40	10.34	0.01	9.83	0.01	9.70	0.01
					60	10.20	0.01	9.71	0.01	9.57	0.01
					80	10.13	0.02	9.66	0.02	9.52	0.02
					100	10.10	0.02	9.63	0.02	9.49	0.03
					120	10.08	0.03	9.60	0.03	9.47	0.04
					140	10.04	0.04	9.58	0.04	9.41	0.05
					160	9.98	0.05	9.52	0.05	9.31	0.05



Table 6—Continued

Cluster ID	$\alpha_{2000}$	$\delta_{2000}$	$d''$	Flag	$R''$	$J$	$J_{err}$	$H$	$H_{err}$	$K$	$K_{err}$
					180	9.97	0.06	9.52	0.07	9.26	0.07
					200	9.94	0.07	9.49	0.08	9.17	0.08
NGC1898	05:16:41.2	-69:39:24.8	3.5	AAA	20	10.92	0.01	10.65	0.02	10.26	0.01
					40	10.11	0.02	9.61	0.02	9.37	0.02
					60	9.61	0.02	9.23	0.03	9.02	0.03
					80	9.34	0.03	8.96	0.04	8.86	0.05
					100	9.23	0.04	8.81	0.06	8.70	0.06
					120	9.15	0.06	8.70	0.08	8.59	0.08
					140	9.04	0.07	8.55	0.09	8.46	0.10
					160	8.93	0.09	8.43	0.11	8.37	0.12
					180	8.80	0.10	8.27	0.12	8.24	0.14
					200	8.68	0.11	8.15	0.13	8.11	0.15
NGC1916	05:18:37.1	-69:24:23.7	9.5	AAA	20	8.82	0.01	8.31	0.01	8.07	0.01
					40	8.40	0.01	7.96	0.01	7.71	0.01
					60	8.22	0.02	7.77	0.01	7.53	0.01
					80	8.11	0.02	7.63	0.02	7.40	0.02
					100	8.04	0.03	7.57	0.03	7.34	0.03
					120	7.97	0.04	7.51	0.04	7.28	0.04
					140	7.91	0.05	7.38	0.05	7.24	0.05
					160	7.86	0.06	7.31	0.06	7.15	0.06
					180	7.80	0.07	7.26	0.07	7.10	0.07
					200	7.74	0.08	7.20	0.08	7.04	0.09
NGC1939	05:21:25.9	-69:56:55.3	5.5	BBA	20	11.03	0.01	10.66	0.01	10.55	0.01
					40	10.30	0.02	9.84	0.02	9.78	0.02
					60	9.98	0.03	9.52	0.03	9.39	0.03
					80	9.80	0.04	9.30	0.04	9.20	0.05
					100	9.68	0.05	9.18	0.06	9.14	0.07
					120	9.54	0.06	9.02	0.07	8.94	0.08
					140	9.35	0.07	8.89	0.08	8.81	0.10
					160	9.26	0.09	8.80	0.10	8.70	0.12
					180	9.13	0.10	8.66	0.11	8.56	0.13
					200	9.05	0.11	8.57	0.13	8.42	0.14

Table 6—Continued

Cluster ID	$\alpha_{2000}$	$\delta_{2000}$	$d''$	Flag	$R''$	$J$	$J_{err}$	$H$	$H_{err}$	$K$	$K_{err}$
NGC1987	05:27:18.1	-70:44:06.1	7	BBA	20	11.05	0.01	10.30	0.01	10.05	0.01
					40	10.66	0.01	9.99	0.01	9.73	0.01
					60	10.16	0.02	9.48	0.01	9.04	0.01
					80	9.96	0.02	9.23	0.02	8.89	0.02
					100	9.89	0.03	9.18	0.03	8.84	0.02
					120	9.69	0.04	9.00	0.03	8.66	0.03
					140	9.52	0.04	8.93	0.04	8.42	0.03
					160	9.46	0.05	8.81	0.05	8.36	0.04
					180	9.40	0.06	8.76	0.06	8.34	0.05
					200	9.32	0.07	8.70	0.07	8.29	0.06
NGC1984	05:27:40.0	-69:08:02.5	6	AAB	20	8.95	0.01	8.39	0.01	8.10	0.01
					40	8.84	0.01	8.34	0.01	8.05	0.01
					60	8.78	0.02	8.31	0.02	8.02	0.03
					80	8.76	0.03	8.30	0.04	8.00	0.05
					100	8.73	0.05	8.30	0.06	7.98	0.07
					120	8.15	0.04	7.56	0.04	7.26	0.05
					140	8.10	0.05	7.52	0.06	7.20	0.07
					160	8.09	0.07	7.52	0.07	7.19	0.09
180	8.08	0.09	7.52	0.09	7.21	0.11					
HODGE14	05:28:38.2	-73:37:44.9	3.5	AAA	20	13.19	0.02	12.35	0.02	12.48	0.03
					40	12.41	0.02	11.72	0.02	11.76	0.03
					60	12.08	0.03	11.40	0.03	11.47	0.04
					80	11.85	0.03	11.19	0.04	11.31	0.05
					100	11.75	0.04	10.98	0.05	11.06	0.06
					120	11.59	0.05	10.87	0.06	10.90	0.08
					140	11.46	0.07	10.77	0.07	10.76	0.09
					160	11.42	0.08	10.70	0.09	10.75	0.12
					180	11.22	0.09	10.68	0.11	10.54	0.12
200	11.21	0.11	10.60	0.13	10.47	0.14					
NGC1978	05:28:44.8	-66:14:08.2	3	BBA	20	10.02	0.01	9.22	0.01	8.85	0.01
					40	9.10	0.01	8.37	0.01	8.09	0.01
					60	8.74	0.01	8.04	0.01	7.81	0.01

Table 6—Continued

Cluster ID	$\alpha_{2000}$	$\delta_{2000}$	$d''$	Flag	$R''$	$J$	$J_{err}$	$H$	$H_{err}$	$K$	$K_{err}$
					80	8.50	0.01	7.81	0.02	7.60	0.01
					100	8.34	0.01	7.66	0.02	7.45	0.01
					120	8.23	0.01	7.57	0.03	7.30	0.01
					140	8.16	0.02	7.51	0.04	7.25	0.01
					160	8.07	0.02	7.41	0.05	7.18	0.02
					180	8.03	0.02	7.37	0.06	7.14	0.02
					200	8.00	0.03	7.35	0.07	7.14	0.03
NGC2005	05:30:10.0	-69:45:07.8	5.5	AAB	20	10.07	0.01	9.52	0.01	9.80	0.01
					40	9.66	0.02	9.17	0.02	9.32	0.02
					60	9.51	0.03	8.96	0.04	9.15	0.04
					80	9.43	0.04	8.85	0.06	9.04	0.06
					100	9.33	0.06	8.75	0.08	8.92	0.08
					120	9.27	0.08	8.65	0.10	8.85	0.11
					140	9.23	0.11	8.58	0.14	8.80	0.15
NGC2004	05:30:41.6	-67:17:14.6	11	AAA	20	8.58	0.01	7.84	0.01	7.57	0.01
					40	8.10	0.01	7.39	0.01	7.12	0.01
					60	7.87	0.01	7.17	0.01	6.89	0.01
					80	7.65	0.01	6.96	0.01	6.69	0.01
					100	7.32	0.02	6.62	0.01	6.36	0.01
					120	7.27	0.02	6.57	0.02	6.30	0.02
					140	7.15	0.02	6.45	0.02	6.19	0.02
					160	7.14	0.03	6.44	0.03	6.19	0.03
					180	7.12	0.03	6.44	0.03	6.18	0.04
					200	7.10	0.04	6.43	0.04	6.18	0.05
NGC2019	05:31:56.0	-70:09:33.4	2	AAA	20	9.80	0.01	9.28	0.01	9.21	0.01
					40	9.29	0.01	8.84	0.01	8.73	0.01
					60	9.10	0.02	8.65	0.02	8.54	0.02
					80	8.94	0.02	8.57	0.02	8.46	0.03
					100	8.84	0.03	8.52	0.03	8.39	0.04
					120	8.77	0.03	8.46	0.05	8.31	0.05
					140	8.69	0.04	8.36	0.06	8.19	0.06
					160	8.58	0.05	8.20	0.07	8.14	0.08

Table 6—Continued

Cluster ID	$\alpha_{2000}$	$\delta_{2000}$	$d''$	Flag	$R''$	$J$	$Jerr$	$H$	$Herr$	$K$	$Kerr$
					180	8.52	0.06	8.13	0.08	8.07	0.10
					200	8.47	0.07	7.97	0.09	7.86	0.10
NGC2011	05:32:19.0	-67:31:24.9	8	AAA	20	9.17	0.01	8.37	0.01	8.05	0.01
					40	8.76	0.01	8.03	0.01	7.72	0.01
					60	8.48	0.01	7.75	0.01	7.46	0.01
					80	8.46	0.02	7.74	0.01	7.45	0.01
					100	8.42	0.02	7.71	0.01	7.45	0.02
					120	8.40	0.03	7.68	0.02	7.42	0.02
					140	8.31	0.03	7.63	0.02	7.38	0.03
					160	7.83	0.03	7.11	0.02	6.82	0.02
					180	7.68	0.03	6.96	0.02	6.68	0.02
					200	7.64	0.03	6.94	0.03	6.66	0.03
HODGE4	05:32:25.0	-64:44:02.1	8	AAA	20	13.25	0.02	12.94	0.03	12.63	0.03
					40	12.01	0.02	11.66	0.03	11.36	0.03
					60	11.32	0.02	10.85	0.02	10.71	0.03
					80	11.05	0.03	10.63	0.03	10.47	0.04
					100	10.83	0.04	10.40	0.04	10.28	0.05
					120	10.74	0.05	10.32	0.06	10.22	0.07
					140	10.63	0.06	10.20	0.07	10.12	0.08
					160	10.59	0.08	10.15	0.08	10.15	0.11
					180	10.53	0.09	10.07	0.10	10.08	0.13
					200	10.48	0.11	10.06	0.12	10.04	0.16
NGC2031	05:33:41.4	-70:59:12.8	3	AAB	20	10.82	0.01	10.10	0.01	10.43	0.01
					40	9.55	0.01	8.78	0.01	8.64	0.01
					60	9.40	0.01	8.68	0.01	8.55	0.01
					80	9.29	0.02	8.60	0.02	8.48	0.02
					100	9.18	0.02	8.49	0.02	8.38	0.02
					120	9.09	0.03	8.43	0.03	8.30	0.03
					140	8.98	0.03	8.31	0.03	8.19	0.04
					160	8.85	0.04	8.18	0.04	8.04	0.04
					170	8.80	0.04	8.14	0.04	7.99	0.04
NGC2100	05:42:08.0	-69:12:46.9	6	AAB	20	9.49	0.01	8.88	0.01	8.64	0.01

Table 6—Continued

Cluster ID	$\alpha_{2000}$	$\delta_{2000}$	$d''$	Flag	$R''$	$J$	$Jerr$	$H$	$Herr$	$K$	$Kerr$
					40	8.21	0.01	7.51	0.01	7.19	0.01
					60	7.64	0.01	6.94	0.01	6.64	0.01
					80	7.47	0.02	6.76	0.01	6.46	0.01
					100	7.27	0.02	6.57	0.01	6.29	0.01
					120	7.23	0.02	6.55	0.02	6.27	0.02
					140	7.05	0.02	6.35	0.02	6.08	0.02
					150	7.04	0.03	6.35	0.02	6.07	0.03
SL663	05:42:30.2	-65:21:38.8	12	AAA	20	13.86	0.04	13.63	0.06	13.19	0.06
					40	12.34	0.03	12.14	0.05	11.84	0.05
					60	11.22	0.02	11.08	0.04	11.02	0.04
					80	11.09	0.04	10.94	0.06	10.92	0.07
					100	10.95	0.05	10.81	0.08	10.76	0.09
					120	10.82	0.06	10.63	0.10	10.53	0.11
					140	10.78	0.08	10.50	0.12	10.20	0.11
					160	10.76	0.10	10.40	0.14	10.11	0.13
					180	10.74	0.13	10.38	0.18	10.07	0.16
					200	10.63	0.14	10.37	0.22	10.04	0.19
NGC2121	05:48:11.9	-71:28:42.4	5	AAA	20	12.75	0.03	12.29	0.03	11.91	0.03
					40	11.38	0.03	10.88	0.03	10.27	0.02
					60	10.47	0.03	9.79	0.03	9.22	0.02
					80	9.94	0.03	9.44	0.04	8.99	0.03
					100	9.75	0.04	9.24	0.05	8.85	0.04
					120	9.58	0.05	9.06	0.06	8.65	0.05
					140	9.47	0.06	8.96	0.07	8.54	0.06
					160	9.38	0.07	8.84	0.08	8.44	0.07
					180	9.14	0.07	8.48	0.08	8.15	0.07
					200	9.05	0.08	8.39	0.09	8.07	0.08
NGC2136	05:52:57.3	-69:29:29.3	166	AAB	20	10.17	0.01	9.55	0.01	9.74	0.01
					40	9.49	0.01	8.90	0.01	8.96	0.01
					60	9.29	0.02	8.79	0.01	8.80	0.01
					80	9.20	0.02	8.72	0.02	8.71	0.02
					100	9.06	0.03	8.60	0.03	8.54	0.03

Table 6—Continued

Cluster ID	$\alpha_{2000}$	$\delta_{2000}$	$d''$	Flag	$R''$	$J$	$J_{err}$	$H$	$H_{err}$	$K$	$K_{err}$
					120	9.02	0.04	8.52	0.03	8.46	0.04
					140	8.97	0.05	8.42	0.04	8.32	0.04
					160	8.89	0.06	8.39	0.05	8.28	0.06
					180	8.81	0.07	8.33	0.07	8.23	0.07
					200	8.75	0.08	8.27	0.08	8.15	0.08
NGC2157	05:57:34.5	-69:11:45.2	4.5	ABB	20	10.28	0.01	9.83	0.01	9.64	0.01
					40	9.23	0.01	8.69	0.01	8.53	0.01
					60	9.01	0.01	8.48	0.01	8.34	0.01
					80	8.93	0.02	8.39	0.01	8.26	0.01
					100	8.86	0.02	8.30	0.02	8.18	0.02
					120	8.83	0.03	8.25	0.02	8.15	0.02
					132	8.82	0.04	8.21	0.03	8.13	0.03
NGC2156	05:57:49.6	-68:27:37.9	17	ABA	20	12.34	0.02	11.74	0.02	11.57	0.02
					40	11.61	0.03	11.31	0.04	11.03	0.04
					60	11.32	0.05	11.01	0.06	10.83	0.06
					80	11.13	0.07	10.85	0.10	10.60	0.09
					100	11.06	0.10	10.75	0.14	10.48	0.13
					120	11.00	0.13	10.64	0.18	10.44	0.18
					140	10.84	0.16	10.45	0.21	10.47	0.26
					160	10.69	0.18	10.39	0.26	10.31	0.29
					180	10.64	0.22	10.34	0.32	10.23	0.35
					200	10.60	0.27	10.28	0.39	10.08	0.39
NGC2153	05:57:50.8	-66:23:58.9	9.5	ABB	20	13.55	0.03	13.03	0.03	12.98	0.05
					40	12.77	0.04	12.31	0.05	12.21	0.06
					60	12.61	0.08	12.37	0.10	11.92	0.09
					80	12.47	0.12	12.45	0.18	11.72	0.13
NGC2173	05:57:58.6	-72:58:45.3	9	AAA	20	11.63	0.02	11.15	0.01	10.69	0.01
					40	10.39	0.02	9.75	0.01	9.51	0.01
					60	10.19	0.02	9.59	0.02	9.36	0.02
					80	10.06	0.04	9.44	0.03	9.23	0.03
					100	9.96	0.05	9.35	0.04	9.13	0.04
					120	9.83	0.07	9.19	0.05	8.98	0.05

Table 6—Continued

Cluster ID	$\alpha_{2000}$	$\delta_{2000}$	$d''$	Flag	$R''$	$J$	$J_{err}$	$H$	$H_{err}$	$K$	$K_{err}$
					140	9.78	0.08	9.14	0.07	8.93	0.06
					160	9.72	0.11	9.07	0.08	8.91	0.08
					180	9.68	0.13	9.05	0.10	8.87	0.10
					200	9.66	0.16	9.05	0.13	8.86	0.12
NGC2159	05:58:03.0	-68:37:17.5	34.5	ABA	20	12.17	0.01	12.43	0.02	11.71	0.02
					40	10.70	0.01	10.29	0.01	10.13	0.01
					60	10.54	0.02	10.14	0.02	10.03	0.02
					80	10.44	0.02	10.02	0.02	9.95	0.03
					100	10.36	0.03	9.90	0.03	9.90	0.04
					120	10.30	0.04	9.86	0.05	9.93	0.05
					140	10.19	0.05	9.78	0.06	9.85	0.07
					160	10.14	0.06	9.74	0.07	9.83	0.09
					180	10.02	0.07	9.72	0.09	9.67	0.09
					200	9.97	0.08	9.65	0.11	9.61	0.11
NGC2155	05:58:32.4	-65:28:39.6	6	AAA	20	12.53	0.02	11.93	0.01	11.89	0.02
					40	11.35	0.01	10.69	0.01	10.63	0.02
					60	11.00	0.02	10.33	0.02	10.38	0.02
					80	10.83	0.02	10.18	0.03	10.26	0.04
					100	10.71	0.03	10.05	0.03	10.15	0.05
					120	10.60	0.04	10.01	0.05	10.04	0.06
					140	10.40	0.04	9.85	0.05	9.83	0.07
					160	10.31	0.05	9.79	0.07	9.77	0.09
					180	10.26	0.06	9.79	0.09	9.71	0.11
					200	10.15	0.07	9.55	0.09	9.48	0.11
NGC2164	05:58:54.9	-68:30:52.2	14	ABB	20	10.92	0.01	10.67	0.01	10.67	0.01
					40	9.98	0.01	9.71	0.01	9.74	0.01
					60	9.54	0.01	9.30	0.01	9.24	0.01
					80	9.38	0.01	9.11	0.01	9.04	0.01
					100	9.31	0.01	9.05	0.01	8.98	0.02
					120	9.26	0.02	9.00	0.02	8.91	0.02
					140	9.23	0.02	8.97	0.02	8.84	0.02
					160	9.08	0.02	8.79	0.02	8.66	0.03

Table 6—Continued

Cluster ID	$\alpha_{2000}$	$\delta_{2000}$	$d''$	Flag	$R''$	$J$	$J_{err}$	$H$	$H_{err}$	$K$	$K_{err}$
					180	9.06	0.02	8.77	0.03	8.63	0.03
					184	9.05	0.03	8.77	0.03	8.61	0.03
NGC2172	06:00:05.5	-68:38:17.7	7	ABB	20	12.61	0.02	12.90	0.03	12.17	0.02
					40	11.35	0.02	11.77	0.03	11.09	0.02
					60	11.27	0.02	11.68	0.06	11.01	0.04
					80	11.09	0.03	11.55	0.09	10.98	0.06
					100	10.98	0.05	11.12	0.10	10.74	0.07
					120	10.94	0.06	11.10	0.14	10.70	0.10
					140	10.89	0.08	11.17	0.20	10.59	0.13
					160	10.84	0.10	11.08	0.24	10.57	0.16
					180	10.80	0.12	10.89	0.26	10.54	0.20
					190	10.83	0.14	10.89	0.29	10.56	0.23
NGC2162	06:00:30.0	-63:43:13.2	6	AAA	20	12.10	0.02	11.20	0.01	11.18	0.01
					40	11.15	0.02	10.38	0.02	10.20	0.02
					60	10.91	0.04	10.22	0.03	10.02	0.02
					80	10.77	0.06	10.14	0.04	9.90	0.04
					100	10.62	0.08	10.01	0.06	9.78	0.05
					120	10.55	0.10	9.97	0.08	9.75	0.07
					140	10.48	0.13	9.91	0.11	9.70	0.10
					160	10.40	0.16	9.84	0.13	9.67	0.12
					180	10.35	0.20	9.82	0.17	9.65	0.15
					200	10.33	0.25	9.77	0.20	9.65	0.19
NGC2190	06:01:01.2	-74:43:37.3	9	BBA	20	13.10	0.03	12.68	0.03	12.74	0.04
					40	11.88	0.03	11.32	0.03	11.18	0.03
					60	11.47	0.04	10.87	0.04	10.69	0.04
					80	10.87	0.04	10.04	0.03	9.63	0.02
					100	10.72	0.05	9.90	0.04	9.47	0.03
					120	10.64	0.07	9.85	0.06	9.44	0.05
					140	10.30	0.07	9.52	0.06	9.08	0.04
					160	10.16	0.08	9.43	0.07	9.01	0.05
					180	10.13	0.11	9.41	0.09	8.99	0.07
					200	10.12	0.13	9.40	0.11	9.00	0.08



Table 6—Continued

Cluster ID	$\alpha_{2000}$	$\delta_{2000}$	$d''$	Flag	$R''$	$J$	$Jerr$	$H$	$Herr$	$K$	$Kerr$
ESO121-3	06:02:02.3	-60:31:20.5	3	BBB	20	14.30	0.06	13.14	0.04	13.21	0.05
					40	13.13	0.08	12.21	0.05	12.17	0.06
					60	12.35	0.08	11.60	0.06	11.71	0.08
					80	12.09	0.12	11.51	0.10	11.56	0.12
					100	11.81	0.14	11.23	0.12	11.41	0.16
					120	11.78	0.20	11.18	0.17	11.30	0.21
					140	11.60	0.23	11.11	0.22	11.36	0.31
					160	11.56	0.30	11.11	0.30	11.39	0.43
					180	11.58	0.39	11.23	0.44	11.51	0.65
					200	11.54	0.48	11.33	0.63	11.41	0.77
NGC2203	06:04:41.3	-75:26:11.0	8	BBA	20	11.76	0.02	11.09	0.01	10.90	0.01
					40	10.52	0.02	9.87	0.01	9.72	0.02
					60	10.13	0.02	9.51	0.02	9.36	0.02
					80	9.69	0.03	9.03	0.02	8.84	0.02
					100	9.57	0.04	8.91	0.03	8.72	0.03
					120	9.44	0.05	8.77	0.04	8.56	0.04
					140	9.36	0.06	8.70	0.05	8.48	0.05
					160	9.26	0.07	8.60	0.06	8.38	0.06
					180	9.19	0.09	8.55	0.07	8.32	0.07
					200	8.95	0.09	8.35	0.07	8.15	0.08
NGC2193	06:06:17.3	-65:05:49.5	5	AAA	20	13.15	0.04	12.47	0.03	12.74	0.05
					40	11.78	0.04	11.10	0.03	10.96	0.03
					60	11.07	0.05	10.41	0.04	10.27	0.04
					80	10.77	0.06	10.10	0.05	9.96	0.05
					100	10.59	0.09	9.88	0.07	9.75	0.07
					120	10.50	0.11	9.84	0.10	9.70	0.09
					140	10.40	0.14	9.76	0.12	9.54	0.11
					160	10.36	0.18	9.70	0.15	9.50	0.14
					180	10.35	0.23	9.67	0.19	9.50	0.18
					200	10.33	0.28	9.66	0.23	9.45	0.21
SL842	06:08:14.5	-62:59:22.7	6	AAB	20	12.08	0.02	11.21	0.01	10.94	0.01
					40	11.88	0.03	11.13	0.02	10.85	0.02

Table 6—Continued

Cluster ID	$\alpha_{2000}$	$\delta_{2000}$	$d''$	Flag	$R''$	$J$	$J_{err}$	$H$	$H_{err}$	$K$	$K_{err}$
					60	11.74	0.05	11.11	0.04	10.79	0.03
NGC2209	06:08:34.7	-73:50:09.2	20	ABB	20	13.59	0.06	13.41	0.10	13.26	0.12
					40	12.08	0.06	11.66	0.08	11.31	0.07
					60	10.79	0.04	9.90	0.03	9.38	0.03
					80	10.63	0.06	9.83	0.06	9.32	0.04
					100	10.53	0.09	9.78	0.08	9.28	0.07
					120	10.45	0.12	9.76	0.12	9.26	0.10
					126	10.42	0.13	9.74	0.13	9.25	0.10
NGC2213	06:10:41.9	-71:31:41.2	0	AAB	20	11.02	0.01	10.18	0.01	9.73	0.01
					40	10.54	0.01	9.72	0.01	9.33	0.01
					60	10.40	0.02	9.56	0.01	9.25	0.01
					80	10.28	0.02	9.41	0.02	9.12	0.02
					100	10.15	0.03	9.25	0.02	8.96	0.02
					120	10.10	0.04	9.16	0.03	8.94	0.03
					140	9.93	0.05	8.98	0.03	8.78	0.04
					160	9.86	0.06	8.93	0.04	8.74	0.05
SL855	06:10:52.8	-65:02:38.1	3	ABB	20	14.85	0.15	13.71	0.08	13.66	0.09
NGC2210	06:11:31.2	-69:07:15.5	2.5	AAA	20	10.05	0.01	9.53	0.01	9.43	0.01
					40	9.45	0.01	8.91	0.01	8.83	0.01
					60	9.27	0.01	8.73	0.01	8.68	0.01
					80	9.16	0.01	8.61	0.01	8.57	0.01
					100	9.08	0.02	8.56	0.02	8.50	0.01
					120	9.04	0.02	8.53	0.02	8.48	0.02
					140	9.00	0.03	8.52	0.03	8.47	0.02
					160	8.98	0.03	8.48	0.04	8.41	0.03
					180	8.95	0.04	8.45	0.05	8.38	0.04
					200	8.92	0.05	8.42	0.06	8.35	0.04
NGC2214	06:12:58.5	-68:15:35.4	9	ABB	20	11.00	0.01	10.34	0.01	10.14	0.01
					40	9.93	0.01	9.30	0.01	9.08	0.01
					60	9.76	0.02	9.18	0.01	8.99	0.01
					80	9.52	0.02	8.95	0.02	8.77	0.02
					100	9.41	0.03	8.84	0.03	8.69	0.02

Table 6—Continued

Cluster ID	$\alpha_{2000}$	$\delta_{2000}$	$d''$	Flag	$R''$	$J$	$J_{err}$	$H$	$H_{err}$	$K$	$K_{err}$
					120	9.32	0.04	8.77	0.03	8.61	0.03
					140	9.13	0.05	8.54	0.04	8.38	0.03
					160	8.96	0.06	8.33	0.04	8.18	0.04
					180	8.93	0.07	8.30	0.05	8.15	0.05
					184	8.92	0.07	8.29	0.05	8.14	0.05
LW431	06:13:27.2	-70:41:42.0	2	BBA	20	11.97	0.01	11.15	0.01	10.92	0.01
					40	11.66	0.02	10.94	0.02	10.78	0.02
					60	11.42	0.03	10.81	0.03	10.65	0.03
					80	11.22	0.04	10.75	0.04	10.51	0.04
					100	11.07	0.05	10.70	0.06	10.46	0.06
					120	10.92	0.06	10.65	0.08	10.35	0.07
					140	10.82	0.08	10.59	0.11	10.35	0.10
					160	10.77	0.10	10.55	0.13	10.31	0.12
					180	10.61	0.11	10.36	0.14	10.13	0.13
					200	10.57	0.13	10.36	0.18	10.07	0.16
HODGE11	06:14:22.5	-69:50:46.1	7.5	AAB	20	12.33	0.02	12.03	0.02	11.37	0.02
					40	11.03	0.02	10.54	0.02	10.31	0.02
					60	10.51	0.02	9.91	0.02	9.88	0.02
					80	10.28	0.03	9.70	0.03	9.71	0.03
					100	10.15	0.04	9.57	0.03	9.59	0.04
					120	10.01	0.05	9.45	0.04	9.50	0.05
					140	9.95	0.06	9.38	0.06	9.49	0.07
					160	9.84	0.07	9.29	0.07	9.44	0.09
					180	9.77	0.09	9.20	0.08	9.37	0.11
					196	9.74	0.10	9.13	0.09	9.33	0.12
NGC2231	06:20:42.4	-67:31:04.5	8	AAA	20	11.86	0.01	10.90	0.01	10.54	0.01
					40	11.40	0.02	10.56	0.01	10.24	0.01
					60	11.08	0.04	10.39	0.03	10.06	0.02
					80	10.90	0.05	10.28	0.04	9.97	0.03
					100	10.78	0.07	10.18	0.06	9.88	0.04
					120	10.72	0.10	10.09	0.07	9.83	0.06
					140	10.68	0.13	10.03	0.10	9.80	0.08

Table 6—Continued

Cluster ID	$\alpha_{2000}$	$\delta_{2000}$	$d''$	Flag	$R''$	$J$	$Jerr$	$H$	$Herr$	$K$	$Kerr$
					160	10.63	0.17	10.00	0.12	9.74	0.10
					180	10.53	0.20	9.92	0.15	9.73	0.13
					200	10.47	0.23	9.87	0.17	9.67	0.15
NGC2249	06:25:49.6	-68:55:06.5	6	ABA	20	12.79	0.02	12.60	0.03	12.37	0.03
					40	11.78	0.03	11.56	0.04	11.07	0.03
					60	11.36	0.04	11.00	0.05	10.68	0.04
					80	11.01	0.05	10.54	0.06	10.20	0.05
					100	10.89	0.07	10.40	0.08	10.15	0.07
					120	10.83	0.10	10.31	0.10	10.11	0.09
					140	10.82	0.14	10.26	0.14	10.01	0.11
					160	10.77	0.17	10.18	0.17	9.97	0.15
					180	10.74	0.22	10.10	0.20	9.94	0.18
					200	10.63	0.25	10.09	0.25	9.93	0.23
NGC2257	06:30:12.8	-64:19:36.4	6	AAA	20	13.06	0.02	12.65	0.02	12.70	0.03
					40	11.68	0.02	11.27	0.02	11.19	0.02
					60	11.00	0.02	10.62	0.03	10.52	0.03
					80	10.58	0.03	10.17	0.03	10.07	0.03
					100	10.22	0.03	9.80	0.03	9.69	0.03
					120	10.09	0.04	9.64	0.04	9.54	0.04
					140	9.96	0.04	9.47	0.05	9.43	0.05
					160	9.78	0.05	9.24	0.05	9.22	0.05
					180	9.63	0.05	9.13	0.06	9.11	0.06
					200	9.56	0.06	9.07	0.07	8.98	0.07

–The notes are the same as in Table 5

Table 7. Comparison photometry of NGC152

Filter ID or color	$D''$	$X$	$Y$	offset	mag	err	Persson et al.	
$K_s$	30	348	159	18.5	10.53	$\pm 0.02$	10.95	$\pm 0.03$
$J - K_s$					1.14	$\pm 0.03$	1.07	$\pm 0.05$
$H - K_s$					0.39	$\pm 0.03$	0.27	$\pm 0.05$
$K_s$	60	353	152	13.0	9.54	$\pm 0.01$	9.58	$\pm 0.02$
$J - K_s$					1.07	$\pm 0.02$	1.17	$\pm 0.02$
$H - K_s$					0.38	$\pm 0.01$	0.37	$\pm 0.03$

-Column 1 is the Filter ID or color being compared with the results from Persson et al., the second column is showing the aperture used for that comparison, 3 and 4 are the atlas image coordinates of the recovered aperture centers based on the maximum throughput experiments. The offsets in pixels (or arc seconds) of these positions from the aperture center used in the present work are listed in column 5. Columns 6 and 7 are showing the magnitude or color values measured on the 2MASS images using recovered aperture positions from Persson et al. (1983) and their uncertainties. The corresponding values from Persson et al. transformed into 2MASS magnitude system by the transformation equations of Carpenter (2001) are listed in columns 8 and 9.

Table 8. Comparison photometry of NGC2209

Filter ID or color	$D''$	$X$	$Y$	offset	mag	err	Persson et al.	
$K_s$	30	461	457	17.5	10.04	$\pm 0.02$	10.02	$\pm 0.03$
$J - K_s$					1.68	$\pm 0.03$	1.81	$\pm 0.02$
$H - K_s$					0.67	$\pm 0.03$	0.70	$\pm 0.03$

-The notes are the same as in Table 7

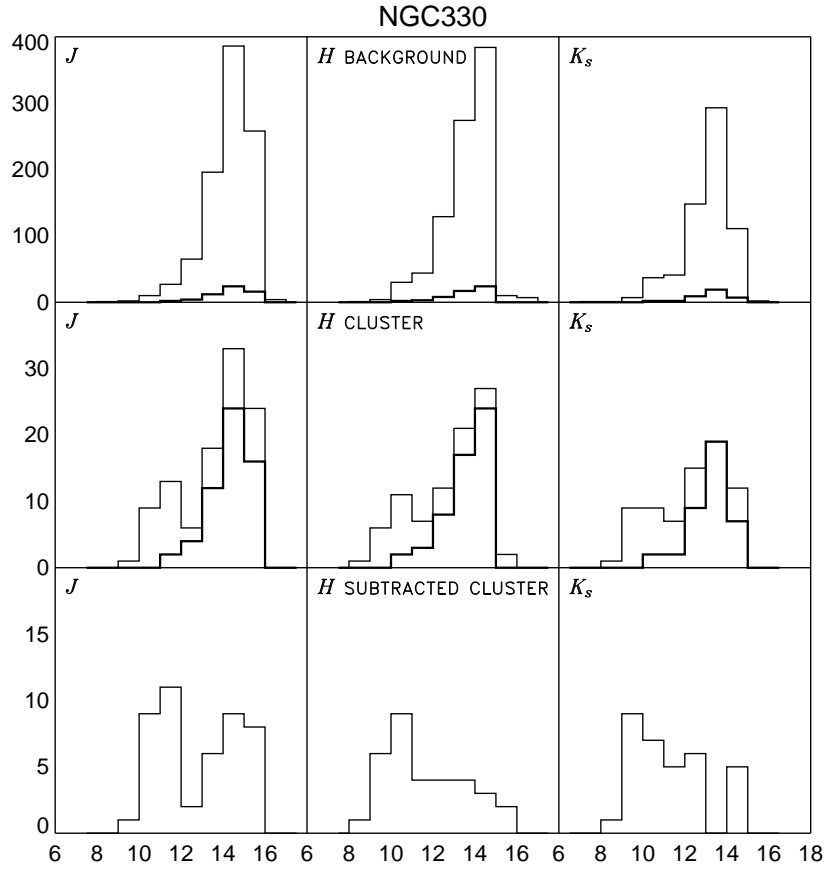


Fig. 3.— Luminosity functions of the background, cluster field and the cluster field after background subtraction from top to bottom. The thick line on the first and second row of panels is representing the background LF scaled to the area of the largest aperture.

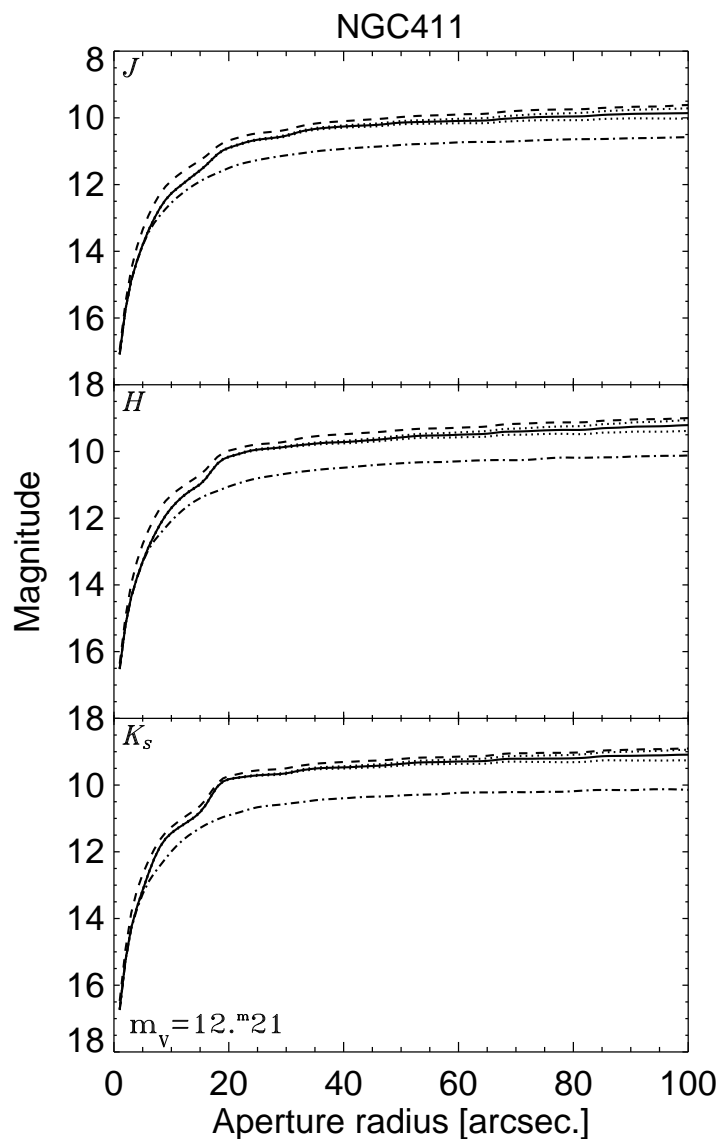


Fig. 4.— Curves of growth in the three 2MASS bands for the SMC cluster NGC411. The dashed curve represents total flux from the object (no background/foreground subtraction applied), dots and dashes are standing for the unresolved component on the Atlas Images. The solid lines are showing the background subtracted curve of growth, and the errors due to the stochastic fluctuations of the background are overplotted with dotted lines. The  $V$  photoelectric magnitude in a  $62''$  diaphragm is taken from Alcaïno (1978).

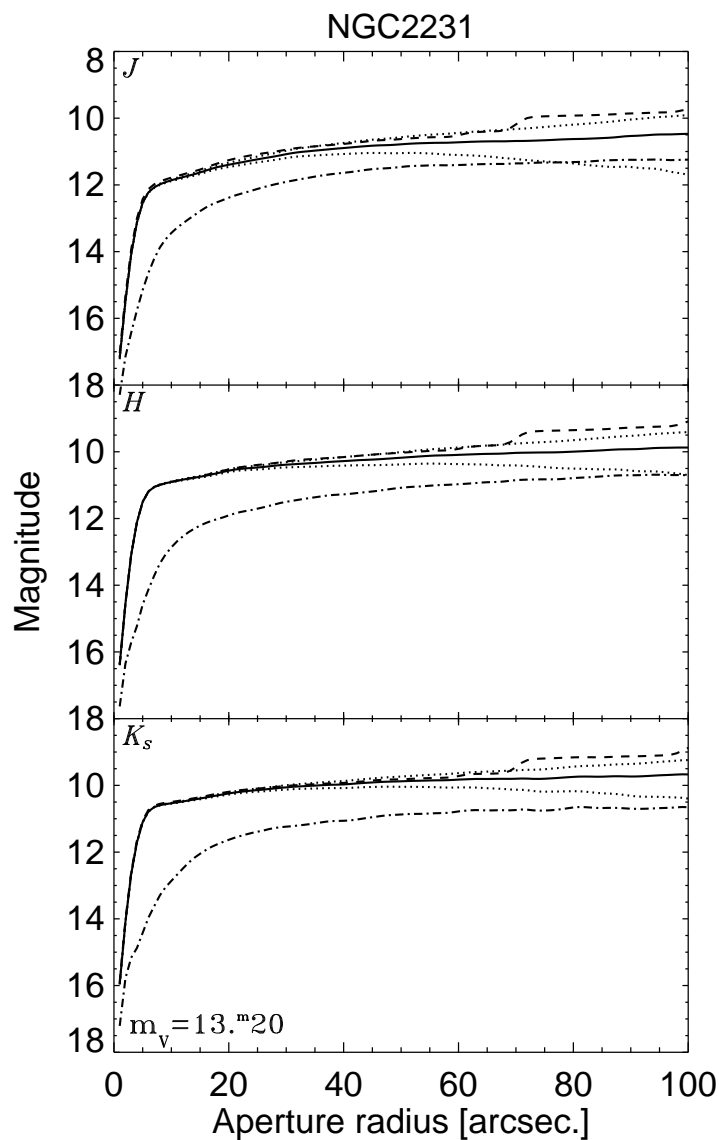


Fig. 5.— Curves of growth in the three 2MASS bands for the LMC cluster NGC2231. The dashed curve represents total flux from the object (no background/foreground subtraction applied), note the clear “bump” due to a foreground star. Solid line is standing for the background subtracted curve of growth, dots and dashes for the unresolved component on the Atlas Images. The errors due to the stochastic fluctuations in the background are overplotted with dotted lines. The values of these errors are quite high because the bright stars in the background field are not excluded from the LF and this is illustrating the possibility of underestimation of the cluster total magnitude. The photoelectric visual magnitude in 44" aperture is taken from van den Bergh (1981).



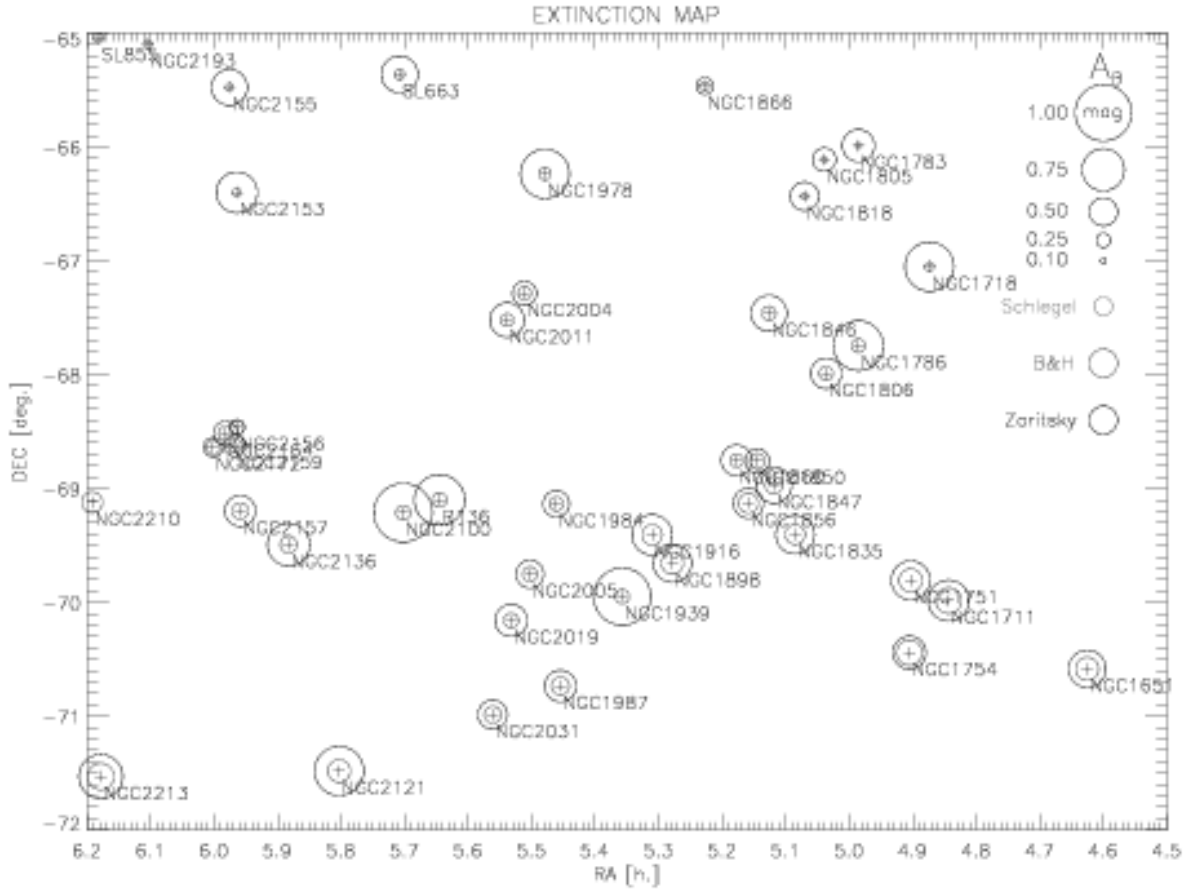


Fig. 6.— Extinction map of the region of LMC where extinction estimations from the different studies are available for all objects in our sample. The values from Burstein & Heiles and Zaritsky et al. are plotted on the map and the extinction for LMC given by Schlegel et al. ( $A_B = 0.32 \pm 0.05$ ) is presented with the corresponding symbol size in the legend.

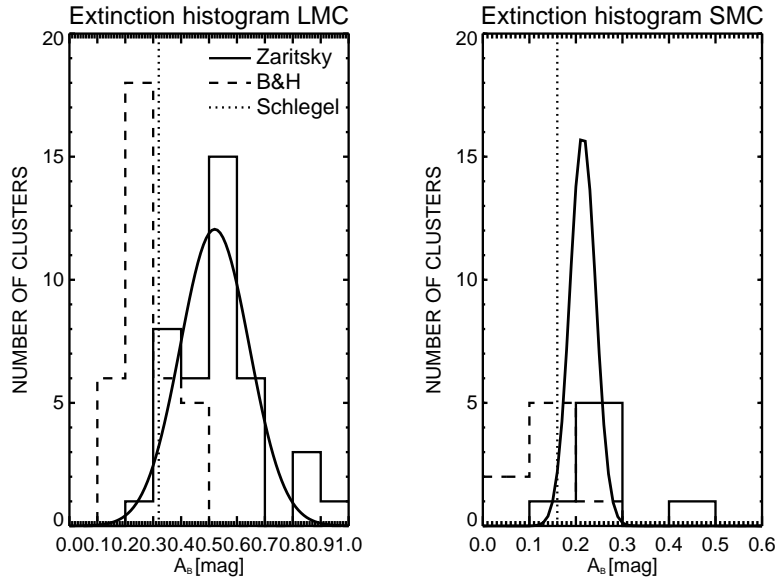


Fig. 7.— Histograms of the extinction values from the studies, Zaritsky et al. and Burstein & Heiles for the objects in the central regions of LMC and SMC. The data is presented in a similar way on the both panels. The Gaussian fit of the MCPS data is overplotted on each histogram. The values from Schlegel et al. for both galaxies are denoted with vertical dotted lines.

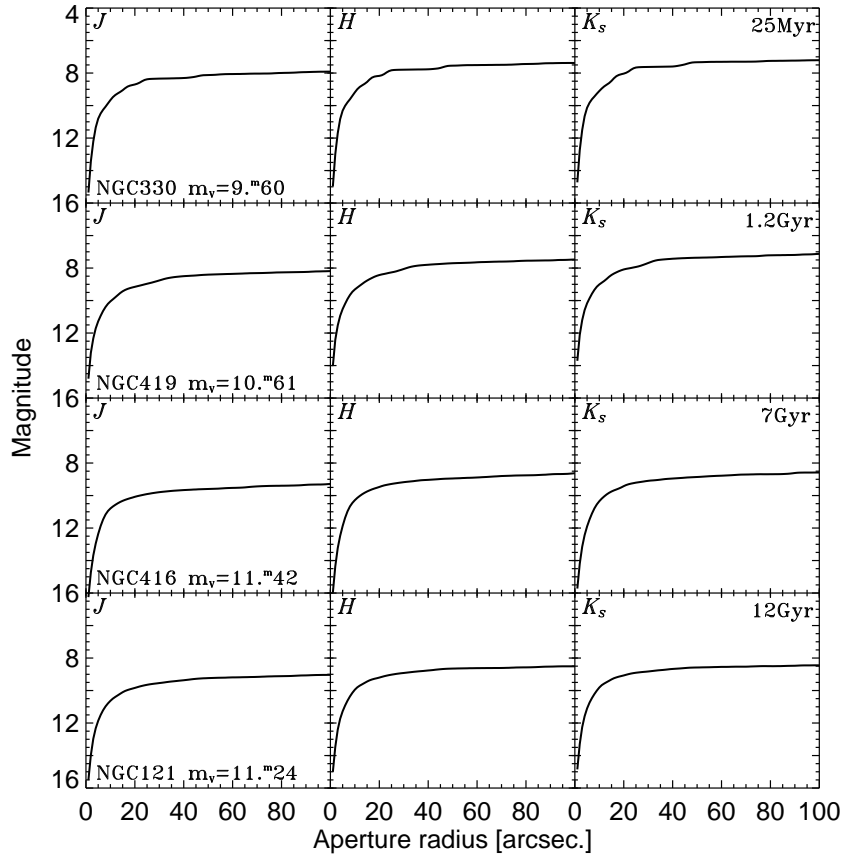


Fig. 8.— Curves of growth for four SMC clusters from our sample. The visual magnitudes are taken from Alcaino (1978). The electrophotometry for all clusters in his study is done by using a  $62''$  aperture. The 2MASS  $J, H$  and  $K_s$  Atlas Images of these clusters with size representable for the diameter of our largest aperture are shown on Figure 1.

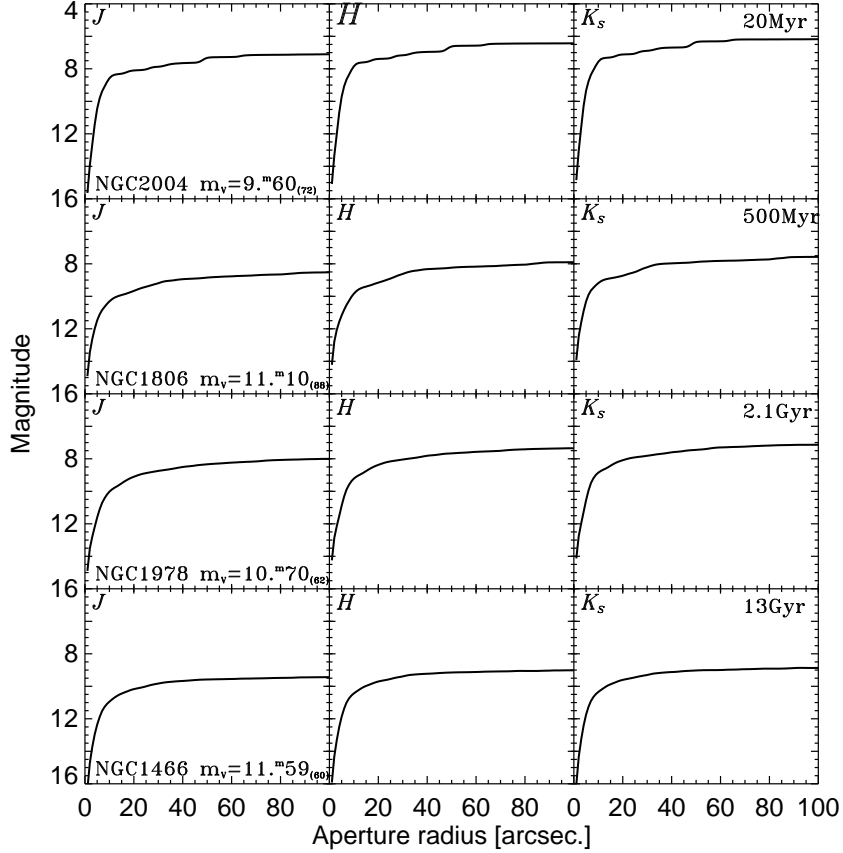


Fig. 9.— Curves of growth for four LMC clusters from our sample. The visual magnitudes are taken from the compilation of Bica et al. (1996). Those data is originating from numerous sources and is not homogeneous by means of detectors and aperture sizes. The apertures used for the measurements of the magnitudes cited on the plots are given in parenthesis. The 2MASS  $J, H$  and  $K_s$  Atlas Images of these clusters with size representable for the diameter of our largest aperture are shown on Figure 2.

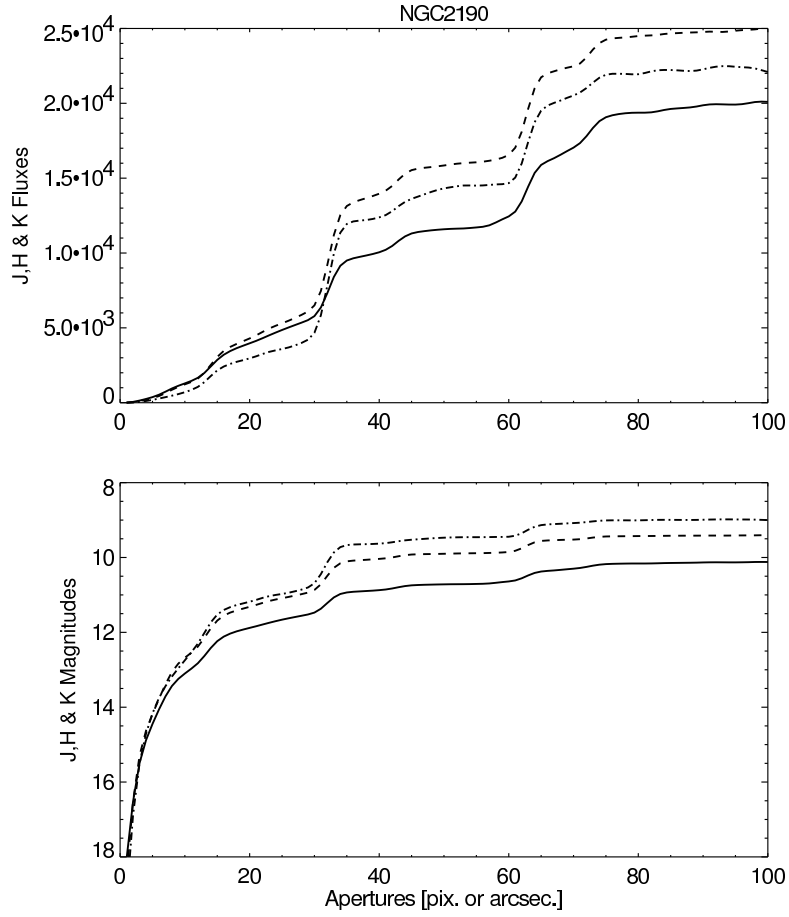


Fig. 10.— Curves of growth in flux units (upper pannel) and magnitudes (lower pannel) for the LMC cluster NGC2190 affected by carbon stars. Note the features around  $r \sim 30''$  and  $60''$  and the steep increase of the flux when the carbon stars are entering into the aperture.

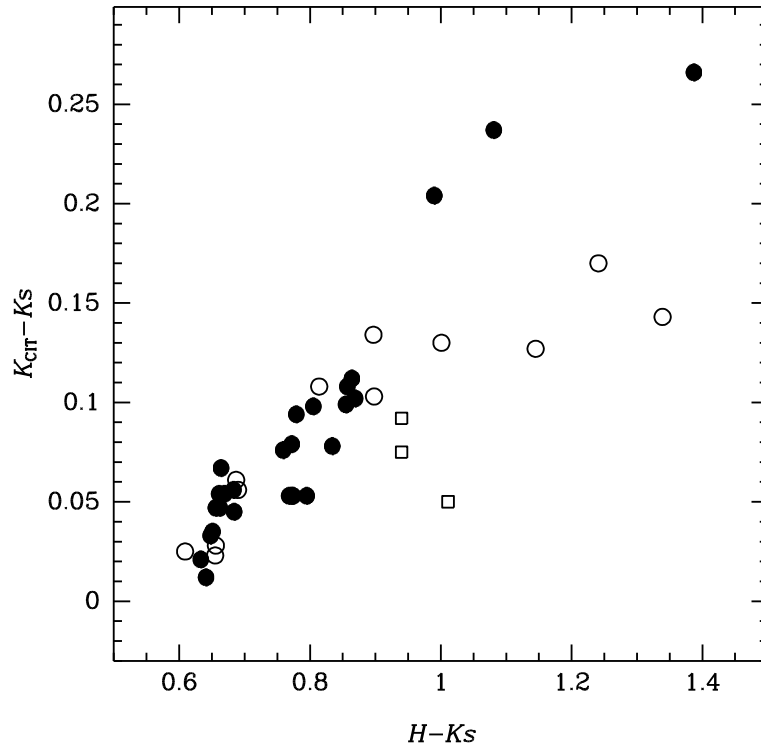


Fig. 11.— Relation between  $H - K_s$  and  $K_{\text{CIT}} - K_s$  for flux-calibrated spectra of late-type stars taken from Lançon & Rocca-Volmerange (1992). Filled circles represent data of giants of spectral types G5III to M8III, open circles represent data of supergiants of spectral types G2I – M7I, and open squares represent data of carbon stars. Note that any difference in calibration from  $K_{\text{CIT}}$  to  $K_s$  between the different spectral types is insignificant for  $H - K_s < 0.9$ .

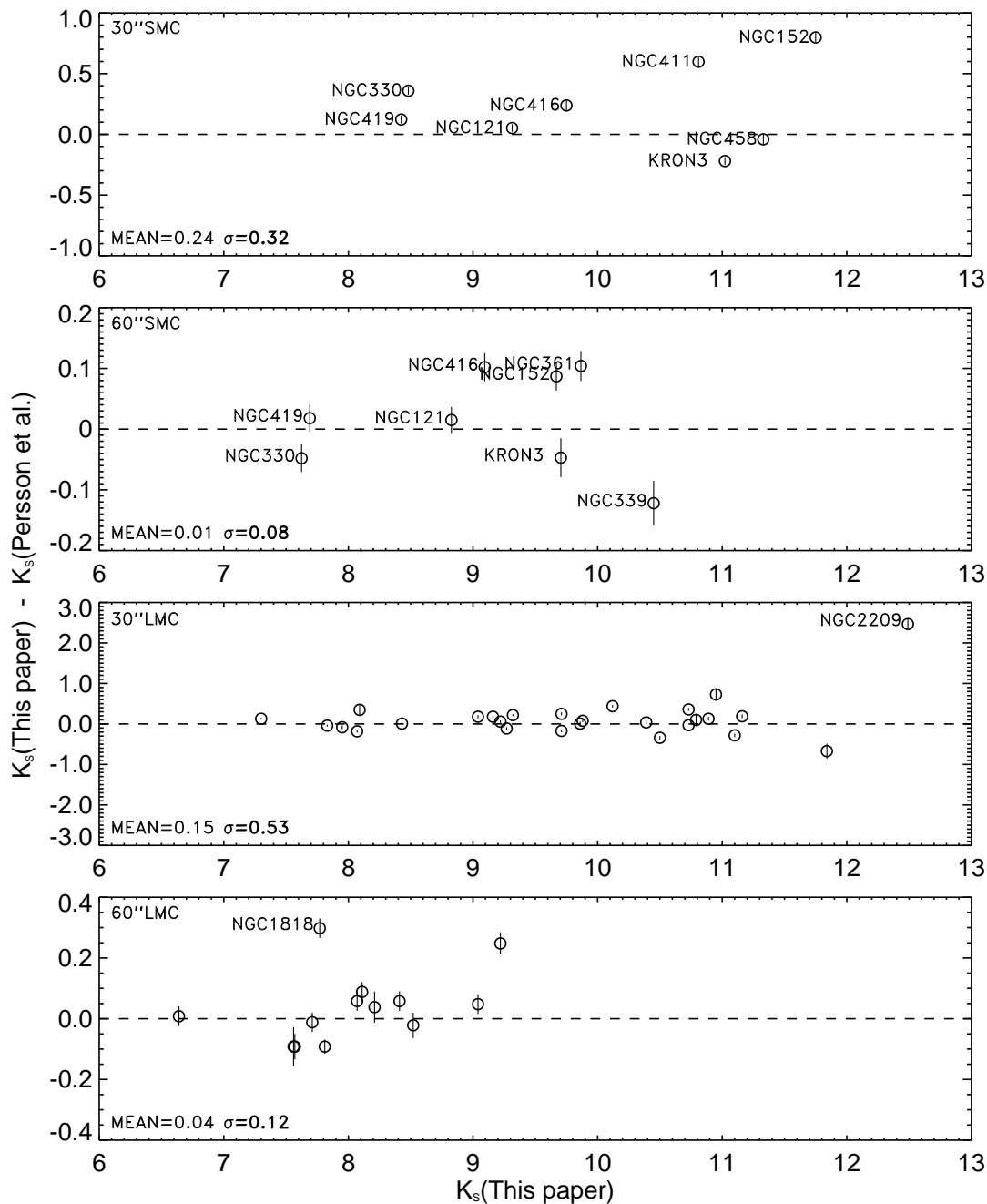


Fig. 12.— Comparison of our 2MASS  $K_s$  band photometry for LMC and SMC clusters with the results of Persson et al. (1983). The dashed line is the one-to-one relation.

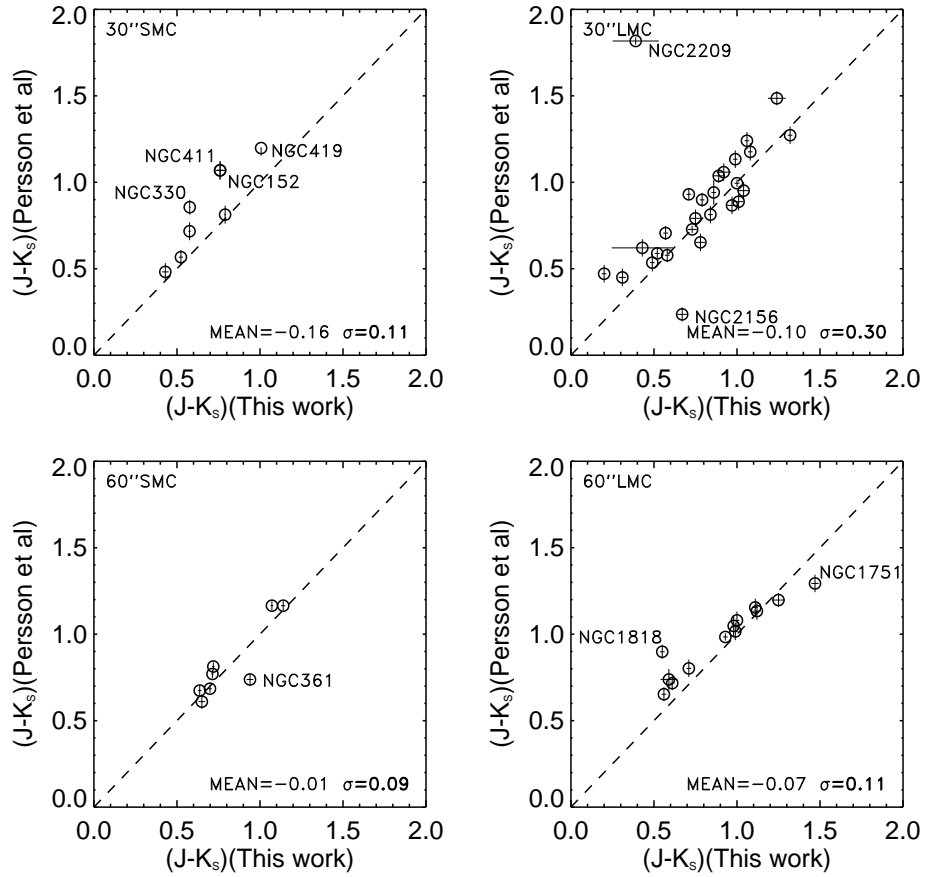


Fig. 13.— Comparison of our 2MASS  $J - K$  colors for LMC and SMC clusters with Person et al. (1983). The dashed line is the one-to-one relation.



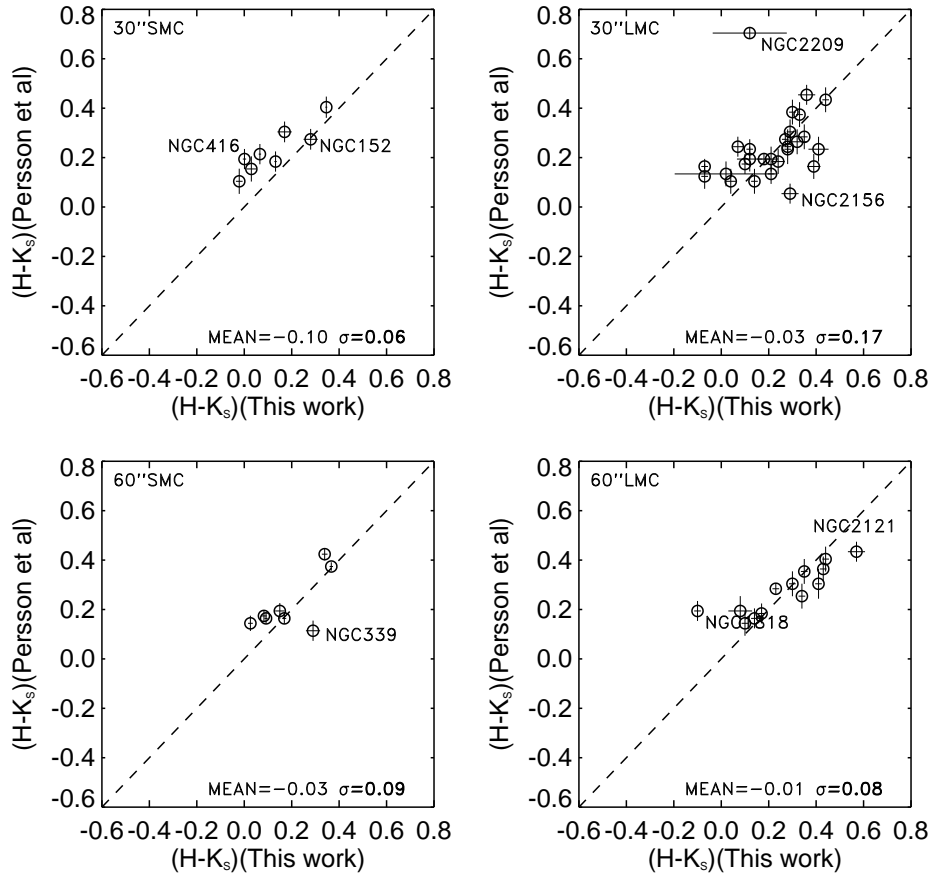


Fig. 14.— Comparison of our 2MASS  $H - K$  colors for LMC and SMC clusters with Persson et al. (1983). The dashed line is the one-to-one relation.

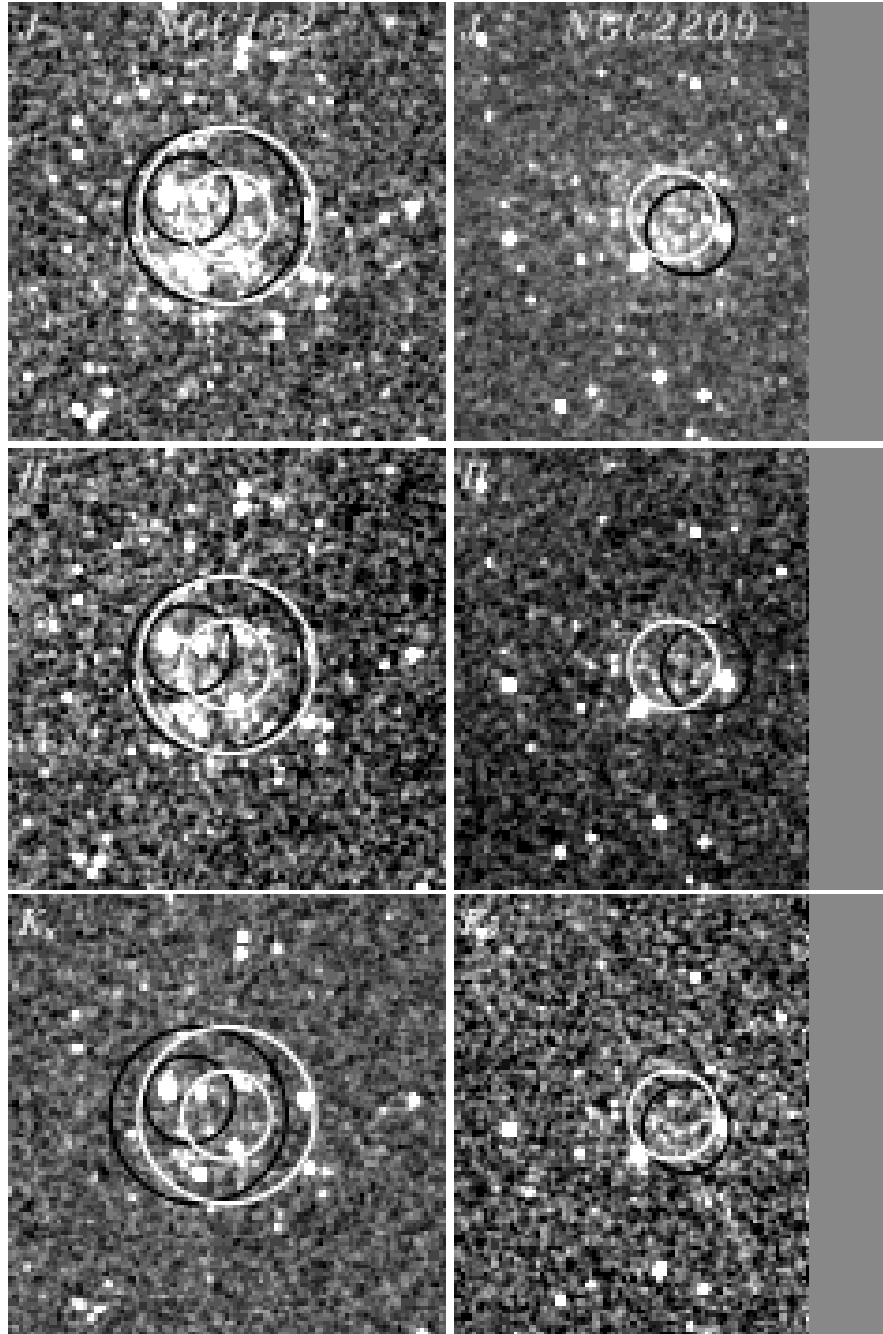


Fig. 15.— 2MASS images of NGC152 and NGC2209. North is up and East is to the left. The images are centered on the positions of our apertures and the size of each one is  $200''$ square. The grey part on the left set of pannels indicate that the object is close to the edge of the Atlas Image. The reproduced apertures of Persson et al. (1983) are plotted in black, and the corresponding apertures from our work are shown in white.

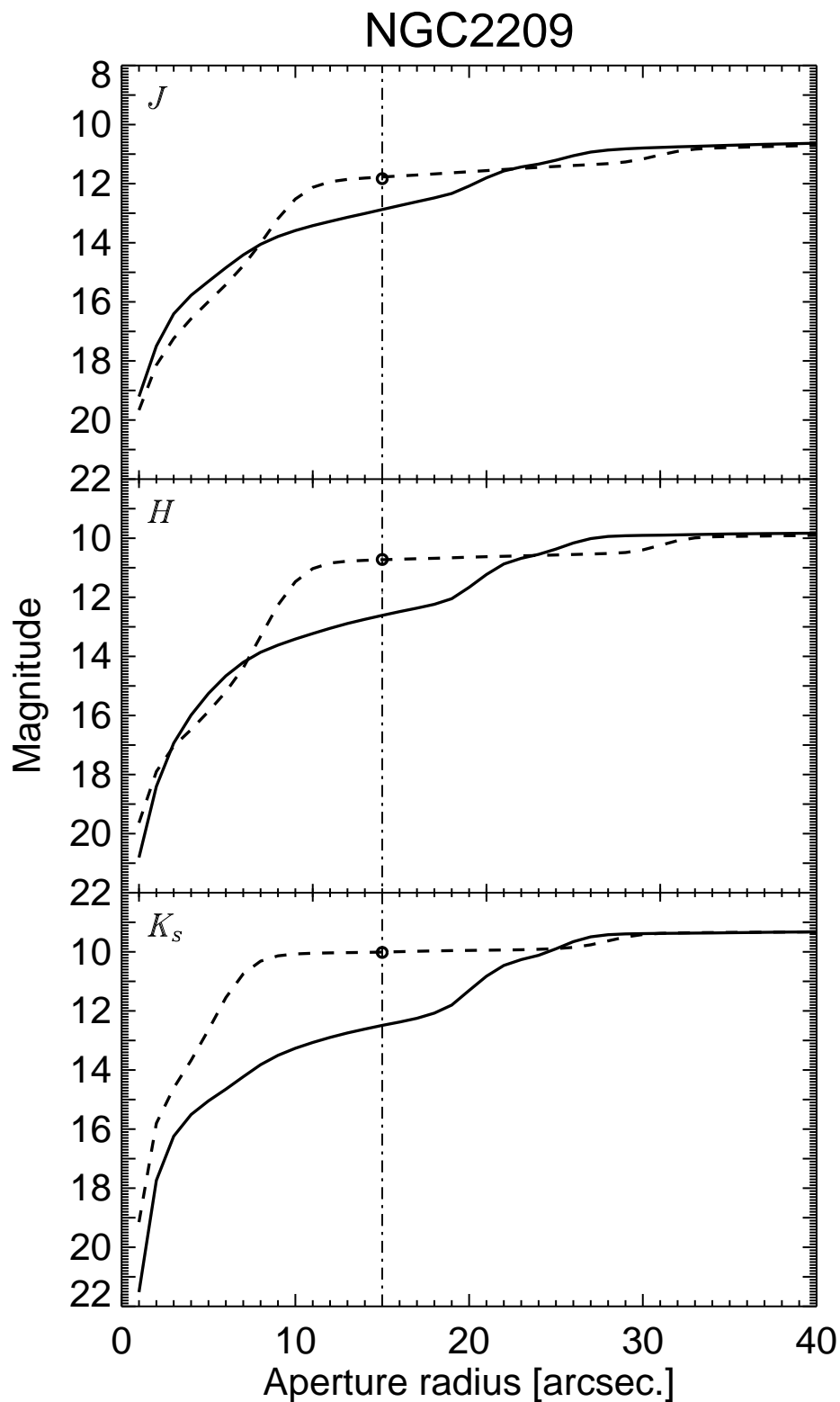


Fig. 16.— *J*, *H* and *K<sub>s</sub>* curves of growth for NGC2209. The solid lines are illustrating our photometry and the dashed lines are standing for the photometry performed with the reproduced centering of Persson et al. (1983). Dot and dashes are showing the 30" aperture diameter. The points are presenting magnitude values from Persson et al. and their error bars are compatible with the point size. Note the good agreement between the measurements

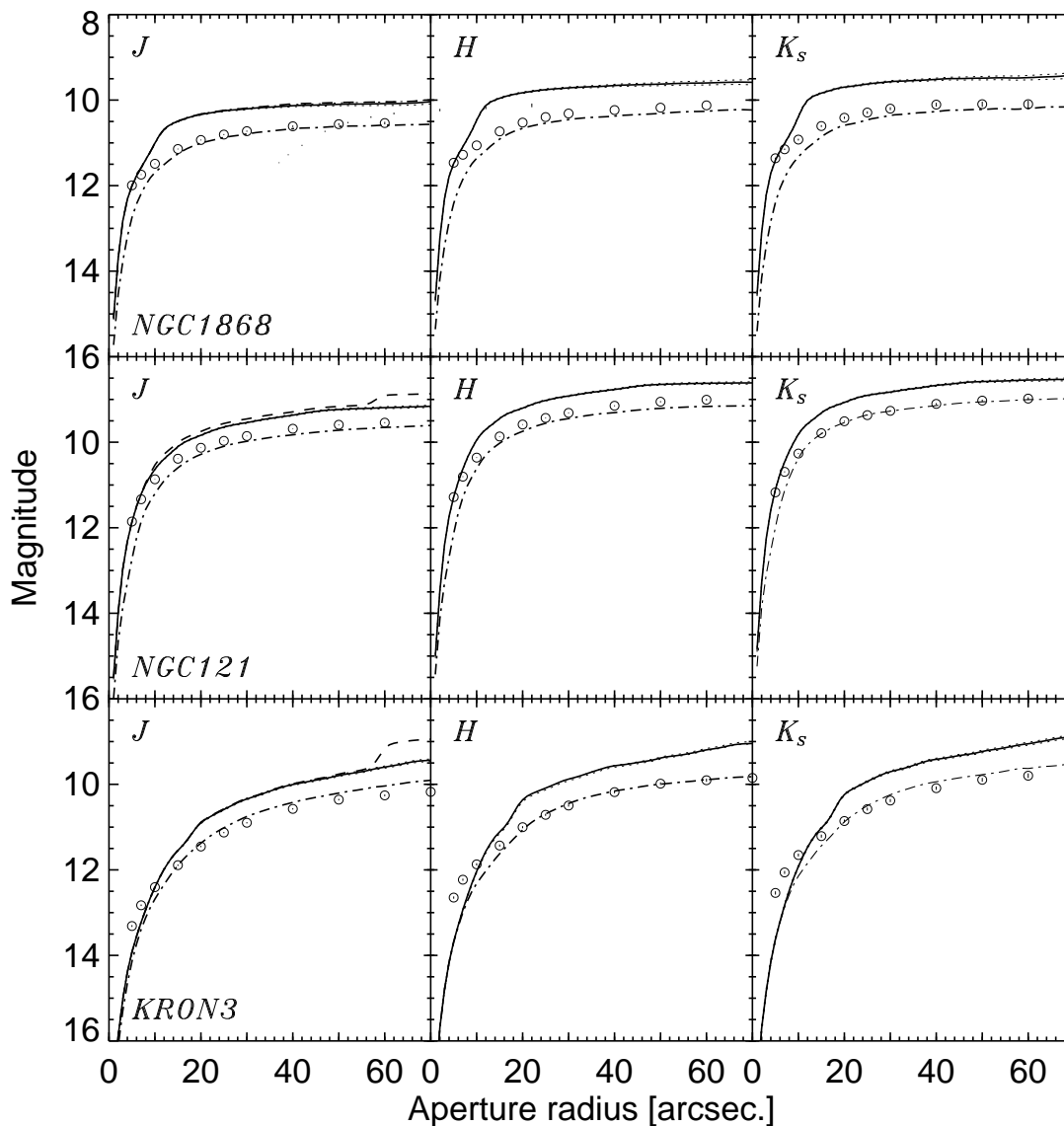


Fig. 17.— Comparison between our photometry (solid lines) and 2MASS XSC values (circles). The errors are compatible to the thickness of the lines. The total signal from the clusters is shown for clarity only in  $J$ . XSC values are in much better agreement with the unresolved component (dots and dashes). The differences in the case of KRON3 could be attributed to the centering of XSC apertures on the peak  $J$  pixel.